



Originally published as:

Sobolev, S. V., Sobolev, A. V., Kuzmin, D. V., Krivolutsкая, N. A., Petrunin, A. G., Arndt, N. T., Radko, V. A., Vasiliev, Y. R. (2011): Linking mantle plumes, large igneous provinces and environmental catastrophes. - *Nature*, 477, 7364, 312-316

DOI: [10.1038/nature10385](https://doi.org/10.1038/nature10385)

Linking mantle plumes, large igneous provinces and environmental catastrophes

Stephan V. Sobolev^{1,2*}, Alexander V. Sobolev^{3,4,5*}, Dmitry V. Kuzmin^{4,6},
Nadezhda A. Krivolutskaya⁵, Alexey G. Petrunin^{1,2}, Nicholas T. Arndt³,
Viktor A. Radko⁷ & Yuri R. Vasiliev⁶

(1) Deutsches GeoForschungsZentrum GFZ, Telegrafenberg, 14473, Potsdam,
Germany;

(2) O.Yu. Schmidt Institute of the Physics of the Earth, Russian Academy of Sciences,
10 ul. B. Gruzinskaya, Moscow, 123995, Russia

(3) ISTERre, CNRS, University Joseph Fourier, Maison des Géosciences, 1381 rue de la
Piscine, BP 53, 38041 Grenoble Cedex 9, France;

(4) Max Planck Institute for Chemistry, 27 J.-J.-Becher-Weg, Mainz, 55128, Germany;

(5) V.I. Vernadsky Institute of Geochemistry and Analytical Chemistry, Russian
Academy of Sciences, 19 ul. Kosygina, Moscow, 119991, Russia;

(6) V.S. Sobolev Institute of Geology and Mineralogy, Siberian Branch of Russian
Academy of Sciences, 3 prosp. Akad. Koptyuga, Novosibirsk, 630090, Russia;

(7) Limited Liability Company «Norilskgeologiya» Norilsk, PO box 889, 663330, Russia

*- These authors contributed equally to this work.

Large igneous provinces (LIPs) are known for their rapid production of enormous volumes of magma (up to several million km³ in less than a million years)¹, for dramatic thinning of the lithosphere^{2,3}, often ending with a continental break-up and for their links to global environmental catastrophes^{4,5}. Despite their importance, controversy surrounds even the basic idea that LIPs form through melting in the heads of thermal mantle plumes^{2,3,6-10}. The Permo-Triassic Siberian Traps¹¹ – the type example and the largest continental LIP^{1,12} (Fig. 1A) – is located on thick cratonic lithosphere^{1,12} and was synchronous with the largest known mass-extinction event¹. However, there is no evidence of pre-magmatic uplift nor of a large lithospheric stretching⁷, as predicted above a plume head^{2,6,9}. Moreover, estimates of magmatic CO₂ degassing from the Siberian Traps are considered insufficient to trigger climatic crises^{13,14,15} leading to the hypothesis that the release of thermogenic gases from the sediment pile caused the mass extinction^{15,16}. Here we present petrological evidence for a large amount (15 wt%) of dense recycled oceanic crust in the head of the plume and develop a thermomechanical model that predicts no pre-magmatic uplift and requires no lithospheric extension. It implies extensive plume melting and heterogeneous erosion of the thick cratonic lithosphere during a few hundred thousand years. The model suggests that massive CO₂ and HCl degassing, mostly from the recycled crust in the plume head, could alone trigger a mass extinction and predicts it happening before the main volcanic phase, in agreement with stratigraphic and geochronological data for the Siberian Traps and other LIPs⁵.

Petrological studies of Siberian Traps and associated alkaline rocks reveal high temperatures (1600-1650°C)^{14,17} in their mantle sources. Olivine compositions in samples from lower units of the Norilsk lava section provide evidence that the mantle source of the Siberian Traps was unusually rich in ancient recycled oceanic crust¹⁴ in agreement with earlier predictions¹⁰. For the main volcanic phase, however, such data were unavailable. Here we report 2500 new olivine analyses and host-rock compositions for 45 basalts covering the main stages of

tholeiitic magmatism in three key localities: the Norilsk area, the Putorana plateau and the Maymecha-Kotuy province (Fig. 1). Almost all olivine compositions possess significantly higher NiO and FeO/MnO than expected for olivine in peridotite-derived magmas (Fig.1b,c supplementary Fig. S1), suggesting a contribution of melts from pyroxenitic sources¹⁸. Alternative explanations of these observations seem less plausible (see Methods for discussion). Our interpretation of the olivine compositions implies that the source of the Siberian Traps contained 10-20 wt.% recycled oceanic crust (*Methods*). More specifically, all lavas erupted during the first stage of magmatic activity (Gudchikhinskaya and earlier suits of the Norilsk area) are depleted in heavy rare earth elements (HREE)^{19,20} indicating residual garnet and derivation within or below the base of thick lithosphere (>130 km)¹⁴. The source of Gudchikhinskaya lavas was likely almost entirely pyroxenitic¹⁴ (Fig. 1b,c,d). Younger magmas are not depleted in HREE indicating formation at shallow depths and dramatic thinning of the lithosphere. Our calculation suggests that these magmas had a near-constant proportion of pyroxenite-derived melt of about 50% (Fig. 1d, table S1 in Supplementary Information) and were strongly contaminated by the continental crust²⁰. Because the main Norilsk section spans less than 1 m.y.¹, it is likely that the lithosphere was thinned in only a few hundred thousand years.

High mantle temperatures over a vast area (Fig.1a) are consistent with the head of a hot mantle plume^{6,9,17}. Based on the petrological constraints we develop a thermomechanical model of the interaction of the plume and lithosphere (see Methods). We assume that the plume arrived below the lithosphere at about 253 Ma (model time 0), perhaps near the northern border of the Siberian Shield, where the hottest melts (meimechites) erupted¹⁷. We further assume that the plume head was hot ($T_p=1600^\circ\text{C}$, 250°C excess temperature) and contained a high content (15 wt.%) of recycled oceanic crust. In our two-dimensional model, we approximate the plume head by a half-circle of 400 km radius located below cratonic lithosphere of variable thickness corresponding to the margin of the

Archean craton (130-250 km of depleted lithosphere and 160-250 km of thermal lithosphere, Fig. S2, Supplementary Information).

The arrival of a large and hot mantle plume head at the base of the lithosphere has been predicted^{6,21} to cause about 0.8-1 km of broad surface uplift per 100°C of plume excess temperature. For a purely thermal plume with an excess temperature of 250°C, we obtain about 2.0 km of surface uplift (Fig. 2a, red curve). However, if a large fraction (15wt%) of dense recycled material is present within the plume, its buoyancy is strongly reduced resulting in little regional uplift (250m) (Fig.2a, black curve). Other processes leading to surface subsidence, such as the plume-induced rise of the 670-km phase boundary²² or the crystallization and evacuation of melts, may easily counteract such a small uplift.

The plume head erodes the lowermost part of the thermal lithosphere and rapidly spreads below the more refractory depleted lithosphere (Fig. 2b). Its ascent leads to progressive melting of recycled eclogitic material in the plume and to the formation of reaction pyroxenite, which melts at depths of 130–180 km, well before the peridotite (Fig. 2e). The early, purely pyroxenite-derived melts yielded the lavas of the Gudchikhinskaya and earlier suites that display the “garnet signature” (Fig. 1d).

We propose that massive intrusion of dykes of Gudchikhinskaya suit imposed compressive stress in the upper brittle part of the lithosphere, “locking” it to the magma transport (Fig. 2b, e shows moment of “locking”). After that, the melt could intrude only into the lower lithosphere (see Methods). The intruding melt cools and crystallizes to dense eclogite. It also strongly heats and weakens the lithosphere, promoting Raleigh-Taylor instabilities⁸. The lower part founders, and the base of the lithosphere is mechanically eroded (Fig. 2c). Enriched in eclogite, the lithospheric material in the boundary layer above the plume escapes

to the sides of the plume and then downwards, allowing plume to ascend (Fig. 2d,f). The plume breaks the lithosphere through in several zones, and in just 100-200 thousand years reaches its minimum depth of about 50 km (Fig. 2d and Fig.S2 in *Supplementary Information*). At this level mafic melts crystallize to a garnet-free assemblage and have a density lower than that of the ambient mantle, thus preventing the formation of Raleigh-Taylor instabilities. This mode of rapid lithosphere destruction does not require regional stretching and matches observations for the Siberian Traps^{7,12}.

The extent of lithospheric destruction depends, among other factors (*Supplementary Information*), on the initial density of mantle lithosphere, which is controlled by its composition (Fig.S3b, *Supplementary Information*). In the case of re-fertilized or moderately depleted mantle lithosphere, the volume of the melt that intrudes into the crust (melt crossed 50 km depth) reaches few percent of the plume volume (Fig. 3a), which leads to substantial melting of the crust and contamination of basalts. Using the proportion of the magma-to-plume volumes from two-dimensional model for a three-dimensional plume head with the radius of 400 km, we estimate the volume of the magma intruded into the crust to be $6-8 \times 10^6 \text{ km}^3$, which is realistic for the Siberian Traps^{1,12}.

In agreement with geochemical data, the model predicts that most magma contain around 50% of pyroxenite-derived melt (Fig.3b, blue curves and symbols) and lack the “garnet signature” because they are generated at depths < 60 km. For the melt generated deeper than 100 km, the model predicts a much higher proportion of pyroxenite melt (75 to 100 %, Fig.3b, red curves), again in agreement with observations (Fig. 3B, red symbols).

Our model allows us to estimate the volume of CO₂ and HCl gases released from the plume. For these calculations, we consider separately the recycled crust and peridotitic components using data from melt inclusions in olivine in

Gudchikhinskaya picrites and mantle peridotite as well as published estimates (Methods). For the composition of recycled crust this yields: HCl=137 ppm; S=135 ppm, H₂O=800ppm and CO₂> 900ppm. The model predicts that most of the CO₂ and HCl in the recycled-crust component of the plume is extracted during its interaction with the lithosphere (Fig. 4a), and a major part is extracted before the main phase of magmatism. For a three-dimensional plume with a radius of 400 km, the mass of extracted CO₂, which mostly comes from the recycled component of the plume, is more than 170 x 10¹² tons. This is several times larger than previous estimates^{13,15} and also exceeds the maximum estimate of the CO₂ released from the magmatic heating of the coals from the Tunguska basin¹⁵.

Our prediction of the mass of CO₂ extracted from the plume is consistent with the amount of CO₂ released during the Permo-Triassic mass-extinction estimated from Ca isotope data²³ (Fig.4a). Moreover, if we use δ¹³C of -12‰ for pyroxenite-derived melt as measured in Koolau (Hawaii) basaltic melt for the source dominated by the recycled crust component²⁴, we can also explain the ¹³C excursion associated with the main mass-extinction event²³ (Methods). Therefore, CO₂ from the plume alone may have triggered the main extinction event. We speculate that low-density and low-viscosity volatiles were the first to penetrate the compressed and mechanically locked crust, triggering the extinction (Fig.4a, upper axis). Alternatively, a sufficient amount of gases may have been released before lithospheric locking, together with the deep-sited magmas of pre-Gudchikhinskaya suits, which could also produce metamorphic gases by magmatic heating of the coals and carbonates. This alternative is supported by recent discovery of coal fly ash in Permian rocks from the Canadian High Arctic immediately before mass extinction, interpreted as a result of combustion of Siberian coal and organic-rich sediments by flood basalts²⁵. In either case, according to our model, the major mass extinction happened before the main phase of flood basalt extrusion. In contrast, most of CO₂ and other gases released by contact metamorphism of carbon- and sulfur-rich sediments, which have been suggested as a trigger for the mass extinction^{15,16}, would be released

during the main phase of magmatism. Precise U/Pb dating of Siberian magmatic units and the Permo-Triassic boundary is required to choose between the two hypotheses. Nonetheless, existing geochronological data^{26,27} and the presence of abundant pyroclastic rocks underlying lavas of the main magmatic phase^{11,19}, support the idea that the major mass extinction predated the main phase of magmatism (see Fig. 4a, upper axis). Additional large amounts of gases released from heated sediments^{15,16} may have been the cause of ¹³C excursions during the later phases of the biotic crisis²⁸.

According to our data and model, the plume also generates a surprisingly large amount of HCl (about 18×10^{12} tons, Fig. 4a), mostly also derived from the recycled component. This quantity of toxic HCl must have been extremely damaging for the terrestrial species and was also sufficient to trigger deadly instability of the stratospheric ozone layer²⁹.

By accepting our viewpoint that degassing of the plume, rather than thermogenic gases from sediments, triggered the biotic crises, we lose an elegant explanation for why the Siberian LIP was so much more damaging to biota than other LIPs of comparable size (Karoo, Parana, North Atlantic) that extruded through other types of sediment or granitic rocks^{15,16}. An alternative explanation is based on the correlation of the intensity of mass extinctions with the age of Phanerozoic LIPs (Fig. 4b), a relationship that can be explained by the temporally different response of the ocean to acidification by the large amounts of released CO₂^{23,30}. In contrast to the Pre-Mid-Mesozoic “Neritan” ocean, the more recent “Cretan” ocean was buffered against acidification by deep-sea unlithified carbonate sediments and was thus much more resistant to acidification^{23,30}. Therefore, CO₂ degassing of a pre-Mid-Mesozoic LIP caused much more severe ocean acidification and mass extinction than later LIPs (Fig. 4b). The only exception is the Deccan LIP and the contemporaneous mass extinction at 65.5 Ma; but in this case, the Chicxulub impact was an additional contributing factor³¹.

Numerical tests (Supplementary Information, Fig. S4-S6) suggest that rapid lithospheric destruction associated with melting in the heads of thermochemical plumes is valid for the large range of plume parameters and lithospheric thicknesses, and therefore may apply not only to the Siberian Traps but also to other LIPs. An absence of prominent pre-magmatic uplift does not argue against a plume origin of LIPs, but may rather point to a high content of recycled crust within the plume. In such cases, other parameters being equal, the model predicts that eclogite-rich plumes caused the most extensive delamination/thinning of the lithosphere thus best preparing it for a possible break-up. They also produced the strongest volcanism and led to the most dramatic climatic consequences.

Another suggestion of our model –that major mass extinctions are triggered by degassing of plume magmas that predate the main magmatic phase – also seems to be consistent with the observations for many LIPs⁵, implying that gas output from plume heads may be much larger than previously thought.

Methods summary

We report new data on 45 representative olivine-bearing samples of Siberian flood basalts from Norilsk, Putorana and Maimecha-Kotui regions (table S1, Supplementary Information). The bulk rocks were crushed, melted and analyzed for major and trace elements by EPMA and LA-ICP-MS at Max-Planck Institute for Chemistry, Mainz, Germany. Olivine phenocrysts (ca 2500 analyses) were analyzed by EPMA using a special high precision protocol¹⁸ at the Max-Planck Institute for Chemistry, Mainz, Germany. Using this new information and published approaches we have estimated the amount of recycled oceanic crust in the sources of basalts and their potential temperatures, and discussed possible alternative models of the source compositions. We further estimate the amounts of H₂O, Cl, S and CO₂ in the recycled oceanic crust and developed a scenario of its degassing during plume-lithosphere interaction.

We model the thermomechanical interaction of the plume and lithosphere by solving numerically a coupled system of momentum, mass and energy conservation equations in two dimensions. We employ non-linear temperature and stress-dependent elasto-visco-plastic rheology, consider pressure- and temperature-dependent melting of a heterogeneous mantle and employ simple models of melt transfer and extraction of volatiles.

Supplementary Information is linked to the online version of the paper at www.nature.com/nature.

References

- ¹ Reichow, M. K. *et al.* The timing and extent of the eruption of the Siberian Traps large igneous province: Implications for the end-Permian environmental crisis. *Earth and Planetary Science Letters* **277**, 9-20, doi:10.1016/j.epsl.2008.09.030 (2009).
- ² White, R. & McKenzie, D. Magmatism at rift zones - the generation of volcanic continental margins and flood basalts. *Journal of Geophysical Research-Solid Earth and Planets* **94**, 7685-7729 (1989).
- ³ Garfunkel, Z. Formation of continental flood volcanism — The perspective of setting of melting, *Lithos* **100**, 49-65 (2008).
- ⁴ Courtillot, V. E. & Renne, P. R. On the ages of flood basalt events. *Comptes Rendus Geoscience* **335**, 113-140, doi:10.1016/s1631-0713(03)00006-3 (2003).
- ⁵ Wignall, P. B. Large igneous provinces and mass extinctions. *Earth-Science Reviews* **53**, 1-33 (2001).
- ⁶ Campbell, I. H. & Griffiths, R. W. Implications of mantle plume structure for the evolution of flood basalts. *Earth and Planetary Science Letters* **99**, 79-93 (1990).
- ⁷ Czamanske, G. K., Gurevitch, A. B., Fedorenko, V. & Simonov, O. Demise of the Siberian plume: Paleogeographic and paleotectonic reconstruction from the prevolcanic and volcanic record, north-central Siberia. *International Geology Review* **40**, 95-115 (1998).
- ⁸ Elkins-Tanton, L. T. & Hager, B. H. Melt intrusion as a trigger for lithospheric foundering and the eruption of the Siberian flood basalts. *Geophysical Research Letters* **27**, 3937-3940 (2000).

- ⁹ Richards, M. A., Duncan, R. A. & Courtillot, V. E. Flood basalts and hot-spot tracks - plume heads and tails. *Science* **246**, 103-107 (1989).
- ¹⁰ Cordery, M. J., Davies, G. F. & Campbell, I. H. Genesis of flood basalts from eclogite-bearing mantle plumes. *Journal of Geophysical Research-Solid Earth* **102**, 20179-20197 (1997).
- ¹¹ Sobolev, V.S.. Petrology of Siberian traps. Transactions, All-Union Arctic Institute, vol. XLIII, L., Izd. GU Sevmorputi. (1936)
- ¹² Dobretsov, N.L., Kirdyashkin, A.A., Kirdyashkin, A.G., Vernikovskiy, V.A. & Gladkov, I.N. Modelling of thermochemical plumes and implications for the origin of the Siberian traps. *Lithos* **100**, 66-92, doi:10.1016/j.lithos.2007.06.025 (2008).
- ¹³ Self, S., Widdowson, M., Thordarson, T. & Jay, A. E. Volatile fluxes during flood basalt eruptions and potential effects on the global environment: A Deccan perspective. *Earth and Planetary Science Letters* **248**, 518-532, doi:10.1016/j.epsl.2006.05.041 (2006).
- ¹⁴ Sobolev, A. V., Krivolutskaya, N. A. & Kuzmin, D. V. Petrology of the parental melts and mantle sources of Siberian trap magmatism. *Petrology* **17**, 253-286, doi:10.1134/s0869591109030047 (2009).
- ¹⁵ Svensen, H. *et al.* Siberian gas venting and the end-Permian environmental crisis. *Earth and Planetary Science Letters* **277**, 490-500, doi:10.1016/j.epsl.2008.11.015 (2009).
- ¹⁶ Ganino, C. & Arndt, N. T. Climate changes caused by degassing of sediments during the emplacement of large igneous provinces. *Geology* **37**, 323-326, doi:10.1130/g25325a.1 (2009).
- ¹⁷ Sobolev, A. V., Sobolev, S. V., Kuzmin, D. V., Malitch, K. N. & Petrunin, A. G. Siberian meimechites: origin and relation to flood basalts and kimberlites. *Russian Geology and Geophysics* **50**, 999-1033, doi:10.1016/j.rgg.2009.11.002 (2009).
- ¹⁸ Sobolev, A. V. *et al.* The amount of recycled crust in sources of mantle-derived melts. *Science* **316**, 412-417, doi:10.1126/science.1138113 (2007).
- ¹⁹ Fedorenko, V. A. *et al.* Petrogenesis of the flood-basalt sequence at Noril'sk, North Central Siberia. *International Geology Review* **38**, 99-135 (1996).
- ²⁰ Wooden, J. L. *et al.* Isotopic and Trace-Element Constraints on Mantle and Crustal Contributions to Siberian Continental Flood Basalts, Norilsk Area, Siberia. *Geochimica Et Cosmochimica Acta* **57**, 3677-3704 (1993).

- 21 Farnetani, C. G. & Richards, M. A. Numerical investigations of the mantle plume initiation model for flood-basalt events. *Journal of Geophysical Research-Solid Earth* **99**, 13813-13833 (1994).
- 22 Leng, W. & Zhong, S. J. Surface subsidence caused by mantle plumes and volcanic loading in large igneous provinces. *Earth and Planetary Science Letters* **291**, 207-214, doi:10.1016/j.epsl.2010.01.015 (2010).
- 23 Payne, J. L. *et al.* Calcium isotope constraints on the end-Permian mass extinction. *Proceedings of the National Academy of Sciences of the United States of America* **107**, 8543-8548, doi:10.1073/pnas.0914065107 (2010).
- 24 Hauri, E. SIMS analysis of volatiles in silicate glasses, 2: isotopes and abundances in Hawaiian melt inclusions. *Chemical Geology* **183**, 115-141 (2002).
- 25 Grasby, S. E., Sanei, H. & Beauchamp, B. Catastrophic dispersion of coal fly ash into oceans during the latest Permian extinction. *Nature Geoscience* **4**, 104-107, doi:10.1038/ngeo1069 (2011).
- 26 Kamo, S. L. *et al.* Rapid eruption of Siberian flood-volcanic rocks and evidence for coincidence with the Permian-Triassic boundary and mass extinction at 251 Ma. *Earth and Planetary Science Letters* **214**, 75-91, doi:10.1016/s0012-821x(03)00347-9 (2003).
- 27 Mundil, R., Palfy, J., Renne, P. R. & Black, P. The Triassic timescale: new constraints and a review of geochronological data. *Geological Society, London, Special Publications* **334**, 41-60, doi:10.1144/SP334.3 (2010).
- 28 Payne, J. L. & Kump, L. R. Evidence for recurrent Early Triassic massive volcanism from quantitative interpretation of carbon isotope fluctuations. *Earth and Planetary Science Letters* **256**, 264-277, doi:10.1016/j.epsl.2007.01.034 (2007).
- 29 Beerling, D. J., Harfoot, M., Lomax, B. & Pyle, J. A. The stability of the stratospheric ozone layer during the end-Permian eruption of the Siberian Traps. *Philosophical Transactions of the Royal Society a-Mathematical Physical and Engineering Sciences* **365**, 1843-1866, doi:10.1098/rsta.2007.2046 (2007).
- 30 Ridgwell, A. A Mid Mesozoic Revolution in the regulation of ocean chemistry. *Marine Geology* **217**, 339-357, doi:10.1016/j.margeo.2004.10.036 (2005).
- 31 Schulte, P. *et al.* The Chicxulub Asteroid Impact and Mass Extinction at the Cretaceous-Paleogene Boundary. *Science* **327**, 1214-1218, doi:10.1126/science.1177265 (2010).

- ³² Masaitis, V. L. Permian and Triassic Volcanism of Siberia: Problems of Dynamic Reconstructions. *Zapiski Vsesouznogo Minearlogicheskogo Obshestva* **112**, 412-425 (1983).
- ³³ White, R. V. & Saunders, A. D. Volcanism, impact and mass extinctions: incredible or credible coincidences? *Lithos* **79**, 299-316, doi:10.1016/j.lithos.2004.09.016 (2005).

Acknowledgments

S.V.S. and A.V.S. are especially grateful to Vladimir Stepanovich Sobolev, who excited their interest in the origin of the Siberian Traps. We are grateful to G.A. Fedorenko for providing data on the Norilsk lavas and valuable discussions. We thank N. Groschopf for help in managing the electron probe microanalyser and O. Kuzmina, N. Svirskaya and T. Shlichkova for sample preparation. Discussions with P. Cardin, N. Dobretsov, E. Galimov, C. Herzberg, A. Hofmann, L. Kogarko, H.-C. Nataf, J. Payne, Y. Podladchikov, I. Ryabchikov, A. Turchyn, and G. Wörner, as well as comments of P. Kelemen and anonymous referees helped improving the clarity of the manuscript. S.V.S. thanks for support the Deutsche Forschungsgemeinschaft (DFG) SPP 1375 SAMPLE (SO 425/4). Study by AVS was funded by ANR, France, Chair of Excellence Grant (ANR-09-CEXC-003-01) and partly supported by a Gauss Professorship in Göttingen University, the Russian Foundation for Basic Research (09-05-01193a), a Russian President grant for leading Russian scientific schools (HIII-3919.2010.5), and an Earth Sciences Department of Russian Academy Grants.

Author Contributions

S.V.S. and A.V.S. provided major contributions to thermomechanical (S.V.S.) and petrological modeling (A.V.S.), to interpretation of data and to writing of the paper. N.A.K. provided geological background and contributed to interpretation, A.G.P. contributed to the thermomechanical modeling at initial stage, N.T.A. contributed to interpretation and writing the paper. D.V.K. processed samples and performed the measurements. N.A.K., V.A.R., Y.R.V. provided carefully selected samples. All authors contributed intellectually to the paper.

Author Information

Reprints and permissions information is available at www.nature.com/reprints. The authors declare no competing financial interests. Readers are welcome to comment on the online version of this article at www.nature.com/nature. Correspondence and requests for materials should be addressed to S.V.S. (stephan@gfz-potsdam.de) or A.V.S. (alexander.sobolev@ujf-grenoble.fr).

Figure captions

Fig. 1. Petrological constraints.

a. Geological map of the Siberian Traps³². Dark green are lavas, light green are tuffs. The dashed black line marks the borders of the province. Red lines outline areas with different magmatic activity: solid indicates maximal, dashed is moderate and dotted is minimal. The three studied regions are Norilsk (N), Putorana plateau (P) and Maymecha-Kotuy province (M). White numbers stand for the potential mantle temperature estimated for lavas of the corresponding areas^{14,17}.

b. FeO/MnO ratios of olivine phenocrysts over normalized-Gd/Yb ratios of host lavas. The blue line marks the pressure that divides “deep” lavas depleted in heavy rare-earth elements from “shallow” lavas. The green oval is the reference for the almost pure shallow peridotitic mantle source and indicates the compositions of olivine and lavas from the mid-ocean ridge (Knipovich Ridge, North Atlantic) with minimum amounts of recycled ocean crust in their sources¹⁸. All olivines are the averages of the highest 3 Fo % of each sample.

c. The proportions of pyroxenite-derived melt in the mixture of pyroxenite- and peridotite-derived melts calculated independently of Mn deficiency (XpxMn) and Ni excess (Xpx Ni)(*Methods*).

d. Integrated lava section for Siberian Traps based on the Norilsk section (*Supplementary Information*). Xpx is the proportion of pyroxenite-derived melt, calculated as the average of XpxMn and XpxNi for high- forsterite olivines and as

XpxMn for low-forsterite olivines, because Xpx Ni for the latter yields systematic overestimation (Fig.1c). Small black dots show lavas of the Norilsk section¹⁹. For abbreviations indicating the lava suites of the Norilsk area and normalization for Dy/Yb ratio (see *Methods*).

Fig. 2. Model.

2a. Maximum pre-magmatic surface uplift atop a spreading mantle plume with an excess temperature of 250°C. The red curve corresponds to the purely thermal plume, and the black curve corresponds to a thermo-chemical plume containing 15 wt% of recycled crust.

2b, c. Temperature distributions (°C) in the model cross-section at model times of 0.15 (b) and 0.5 (c) m.y. The solid line marks the boundary of the depleted lithosphere, and the dashed half-circle denotes the initial shape of the starting plume.

2d. Snapshots of the plume breaking through the lithospheric in the zoom-in domain shown by the white rectangle in figure section f. Colors show concentrations of the pyroxenitic component in the plume or in the crystallized melt.

2e, f. Distribution of the pyroxenite component in the plume or in the crystallized melt in the model cross-section at model times of 0.15 (e) and 0.5 (f) m.y. The solid line marks the boundary of the depleted lithosphere.

Fig. 3. Model predictions.

3a. Evolution in time of a melt volume crossing the 50-km depth and normalized to the volume of the plume. The solid and dashed curves correspond to the models with re-fertilized lithosphere and moderately depleted lithosphere, respectively.

3b. The fraction of pyroxenitic component in basalts of the Norilsk cross-section versus the fraction of the volume of extruded magmas. The blue color corresponds to the “shallow” melts that do not retain a garnet signature, and the red color corresponds to the deep melts that retains a garnet signature. Symbols denote data from olivine compositions; see Fig.1b for the legend. Error bars

correspond to 1 standard deviation of mean of pyroxenite-derived melt proportions estimated independently from Ni excess and Mn deficiency of olivine (Methods and Table S1 in Supplementary Information). The solid and dashed curves show the modeled average melt compositions with re-fertilized and moderately depleted lithosphere, respectively. The grey rectangle shows the range of variation of the model-predicted melt compositions.

Fig. 4. Volatiles production and its consequences for mass extinctions

4a. Modeled CO₂ (left axis) and HCl (right axis) amounts (in terra tones) extracted from the plume versus model time (lower axis). Solid curves show the minimum estimate and dashed curves maximum estimate of CO₂ and HCl extracted from the plume (*Methods*). Grey rectangle shows the estimated range of the released CO₂ during the Permo-Triassic mass extinction²³. Green field shows time dependency of the normalized volume of the magma crossing the 50 km depth, calculated for the re-fertilized lithosphere (Fig. 3a). At the upper axis we show geological time and possible scenario for triggering the Permo-Triassic mass extinction. GBT stands for Gases Break Through. Shown is also U/Pb dating of the extinction event²⁷ and U/Pb dating of main phase Siberian basalts²⁶ and intrusions¹⁵.

4b. Mass extinction intensity (light blue field) with major LIPs (circles) versus geologic time, modified from ref(33), together with the timing of different ocean modes³⁰. Circle colors denote timing of LIPs relative to ocean modes, blue “Cretan” mode and red “Neritan” mode, blue and red together denote transition mode. CAMP and NAMP stand for Central and Northern Atlantic Magmatic Provinces, OJP for Ontong Java and CP for Caribbean Plateaus, CR for Columbian River basalts.

Methods

Samples. Studied samples and their localities are described in the Supplementary Information.

Analytical methods. Olivine grains were manually separated from crushed lavas, then mounted and polished in epoxy. The compositions of olivine were analyzed by Electron Probe Microanalyzer (EPMA) on a *Jeol JXA 8200 SuperProbe* at the Max Planck Institute for Chemistry (Mainz, Germany) at an accelerating voltage of 20 kV and a beam current of 300 nA, following a special procedure which allows 20–30 ppm (two-sigma error) precision and accuracy for Ni, Ca, Mn, Al, Ti, Cr, and Co, and 0.02 mole percent accuracy for the forsterite component in olivine¹⁸.

Bulk rocks were crushed, melted to glass³⁴ then mounted and polished in epoxy. Major and trace elements were determined by EPMA also at the Max Planck Institute for Chemistry. Major-element abundances in glasses were measured at an accelerating voltage of 15 kV and a beam current of 12 nA with a reference sample of natural basaltic glass USNM111240/52 (VG2)³⁵, with a relative error of 1–2%. LA-ICP MS was used to determine trace elements in glasses of melt inclusions and in olivines, on an *ELEMENT-2, Thermo Scientific* mass spectrometer with a *UP-213 New Wave Research* solid-phase laser at the Max Planck Institute for Chemistry, with reference to the KL-2G and NIST 612 standard samples of basaltic glass³⁶.

Proportions of pyroxenite derived melt and recycled crust. We interpret excessive Ni and deficient Mn concentrations in Siberian olivine phenocrysts relative to olivine in peridotite-derived melt as a result of contribution of olivine free pyroxenite lithology in their source^{18,37-39}. The alternative explanations of this phenomenon are briefly discussed in the next section. Relative proportions of pyroxenite and peridotite derived melts were estimated using MnO/FeO (Xpx Mn) and NiO*FeO/MgO (Xpx Ni) ratios³⁸ for each sample using the average composition of most magnesian olivines (defined by olivines with Fo within 3 mol% from a maximum Fo).

Amount of recycled crust in the plume is linked to the proportion of pyroxenite-derived melt by the degree of melting of the eclogite component, the amount of eclogite-derived melt needed to produce hybrid pyroxenite from peridotite, and the degrees of melting of peridotite and pyroxenite^{18,39}. We calculated the

amount of recycled crust in the Siberian plume using the approach of Sobolev et al, (ref 18) and their equation S3, and the following assumptions: a maximum degree of melting of eclogite and pyroxenite of 60%; an average proportion of pyroxenite derived melt in shallow magmas of 46% (Table S1); and melting of peridotite at 50 km depth. The amount of recycled crust is 10 and 20% for 10 and 25% melting of peridotite, respectively.

Alternative models for the source composition for Siberian flood basalts.

Alternative explanations of high Ni/Mg and FeO/MnO ratios in olivine include: (1) effect of clinopyroxene crystallization, (2) an underestimated temperature effect on olivine-melt partition of Ni and (3) contribution of core material to the mantle source. None of these alternatives require a significant role of olivine-free pyroxenite in the mantle source. In addition there are different models for the pyroxenite origin, which may affect our estimation of proportions of pyroxenite in the Siberian plume. These include (4) solid-state reaction of peridotite and recycled crust in the lower mantle and (5) partial reaction between eclogite-derived melt and peridotite. Below we briefly discuss these alternatives.

1. Crystallization of clinopyroxene together with olivine may increase both Ni/Mg and Fe/Mn ratios in olivine. This effect could be particularly important for the low magnesian evolved olivine. However clinopyroxene crystallization can be recognized by low Ca in olivine. In the Supplementary information we show that this is an unlikely scenario for majority of studied olivines, which do not show a significant decrease of Ca concentrations. In particular early clinopyroxene crystallization cannot explain the composition of the olivines from picrites of Gudchikhinskaya formation and Ayan river, which are extremely rich in Ni and deficient in Mn. In addition, melt inclusions in the former¹⁴ and olivines in the latter (Table S3) do not indicate early clinopyroxene crystallization. We conclude that the fractionation of clinopyroxene could not have produced the observed anomalies in the olivine compositions.

2. An underestimated temperature effect on olivine-melt partition coefficient, if present, may increase Ni concentration in the shallow olivine compare to olivine in the deep source due to temperature difference between the sites of generation

and crystallization. This issue has been discussed by A.V. Sobolev et al. [ref 39 and C. Herzberg, [ref 37] who show that any temperature effect additional to compositional one considered in the model of Ni partitioning between melt and olivine used in this study⁴¹ is too small to explain extent of Ni excess observed in Siberian olivines.

3. Contribution of core material to increase Ni /Mg [ref 41] and Fe/ Mn [ref 42] ratios has been discussed before by A.V. Sobolev et al. [ref 18] who show that this explanation is highly unlikely because of a lack of correlation between Ni excess and high Co concentrations in the olivines.

4. Solid-state reaction between recycled crust and peridotite in the lower mantle may produce pyroxenite with composition much closer to peridotite, which in the upper mantle will be transformed to olivine-bearing pyroxenite³⁷. If this lithology exists, it could potentially be the source of parental melts of typical Siberian basalts. However olivine-bearing lithologies could not be the source of deep-sourced lavas like the Gudchikhinskaya formation and Ayan river picrites, whose olivine compositions demonstrate derivation from a dominating olivine-free source. In addition solid-state reactions of the type envisaged by Herzberg will be limited by slow volume diffusion in the mantle⁴³, while production of reaction olivine-free pyroxenite will be restricted only by melt percolation velocity^{18,39}.

5. Incomplete reaction between eclogite-derived melt and peridotite may produce olivine-bearing lithologies⁴⁴, which could be potential sources of the parental melts of typical Siberian traps. However these sources cannot produce Siberian the deep-sourced magmas (see above).

We conclude that while we cannot fully exclude some of proposed alternatives, our explanation of the olivine compositions is based on solid grounds and seems the most plausible.

Potential temperatures. The published potential temperature of 1540°C for the source of Gudchikhinskaya magmas¹⁴ has been corrected for the effect of 40% melting of pyroxenitic source¹⁷, amount of pyroxenite in the plume (15%) and latent heat of melting⁴⁵. The obtained value is about 1600°C. Potential

temperatures for the Maimecha-Kotuy province¹⁷ and Putorana plateau⁴⁶ (see Fig 1A) were obtained for magmas strongly enriched in highly incompatible elements. These magmas originated at low degrees of melting and thus were not corrected for the melting effect.

Amount of volatile elements. The concentrations of volatile elements in the recycled oceanic crust in the Siberian plume were constrained using the compositions of inclusions of uncontaminated melt in early olivine phenocrysts from Gudchikhinskaya magmas. For these magmas it was shown from both olivine and melt compositions that they probably represent melting of pure pyroxenitic source¹⁴. Inclusions in olivine from these magmas have been shown to represent primary melts¹⁴ and thus their concentrations of Cl, S and H₂O can be used to estimate the contents of these volatiles in the mantle source. For the composition of source eclogite, this yields the following values^{14,17}: Cl=137 ppm; S=135 ppm, H₂O=800ppm, after normalization of the values to potassium. In the deep mantle, these amounts of Cl, S and H₂O could reside in chloride⁴⁷, sulfide and garnet or pyroxene respectively. Contrary to Cl, S and H₂O, the amount of CO₂ in relatively shallow melts does not represent the primary concentration due to almost complete degassing at high pressures. Thus for assessment of CO₂ in the recycled oceanic crust we use global estimations of 3000 ppm CO₂ for the bulk 7-km-thick oceanic crust and its maximum outgassing rate through arc volcanism of 70% (ref 48). This gives a conservative minimum estimate of **900** ppm of CO₂ in the deeply recycled oceanic crust. The maximum estimate would be around 1800 ppm using the same initial bulk concentrations of CO₂ and minimal outgassing of 40% (ref 48). In the deep mantle this amount of CO₂ could reside in carbonates or diamond⁴⁷. For our model we use the minimum conservative estimate of CO₂ =900 ppm.

Thermo-mechanical numerical technique. We use a fully coupled thermo-mechanical formulation for the system of momentum, mass and energy conservation equations in 2D with non-linear temperature and stress-dependent elasto-visco-plastic rheology, described in details in ref(49) (for parametrs and procedure for calculating density see in Supplementary Information). Equations are solved numerically using the explicit Lagrangean

FEM technique LAPEX2D ref(50) based on a FLAC algorithm (prototype described in ref(51)) combined with a particle-in-cell approach. All time-dependent fields including full stress tensor are stored at particles.

Melting models. We use a simplified model for batch melting of four components: peridotite, pyroxenite and two eclogites formed through the crystallization of peridotitic and pyroxenitic melts, respectively. Melting temperatures are defined as follows: for peridotite we used the dry batch melting model⁵²; for pyroxenite we use following relation from experiments¹⁸ for dry batch melting of pyroxenite

$$T_m^{Px} = 976 + 12.3P - 0.051P^2 + 663.8X - 611.4X^2 \quad (S2)$$

Where P is pressure in kbar, T is potential temperature in °C and X is melting degree, $0 < X < 0.55$.

For eclogite of both types (peridotite- or pyroxenite-derived) we use following relation approximating experiments⁵³ for dry batch melting of eclogite at 50% melting

$$T_m^e = 1173.4 + 5.78P \text{ at } P < 55 \text{ kbar}; T_m^e = -237.5 + 48.0P - 0.3P^2 \text{ at } 55 < P < 80 \text{ kb} \quad (S3)$$

The melting for each finite element is organized sequentially, beginning with the component with lowest melting temperature (usually eclogite), then usually pyroxenite and finally peridotite. If the current temperature (T) in a finite element exceeds the melting temperature (T_m) of the component that exists in this element, than a certain amount of melt (dC_m) is generated that lowers current temperature to the melting temperature, $dC_m = (T - T_m) * C_p / (\Delta S_m * T)$, where C_p is heat capacity and ΔS_m is entropy of melting, set to 1200 J/kg/K and 400 J/kg/K, respectively, for all components.

Model for melt transfer. We assume that melt transfer within the melting domain occurs much faster than the Raleigh-Taylor instability develops in the lithosphere. This assumption holds if the velocity of melt transfer (V_m) is much higher than H/τ, where H is typical distance of melt transfer and τ is typical time of Raleigh-Taylor instability. With values of H < 50 km, and τ ≈ 50000 years (see

Fig. S2), this assumption is valid if V_m is much higher than 1m/yr. In reality V_m is at least 10 times higher in the upper mantle regions where intensive melting occurs⁵⁴.

If present, the entire melt is assumed to move rapidly upwards within the domain where local temperature is higher than melting temperature. As usual for the melt porous flow, we also assume that it is thermally equilibrating at each element. In practice, at every N-th calculation time-step, for every element we check the melting condition, and move the entire volume of melt (if present) one element upward, recalculating the temperature of that element according to the local energy conservation law.

For the melt in the uppermost elements of the melting domain, we consider two transfer modes. (1) A mode that mimics transfer through fractures. In this case, a fraction or the entire melt, is assumed to move to the surface: in practice is just taken out from the model. (2) A mode of mechanically locked lithosphere. In this case the entire melt from each uppermost element of the melting zone is moved to, and evenly distributed between K elements in the column right above it (usually we take $K=4$) and is assumed to crystallise. Simultaneously, the rheology of melt-accepting lithospheric elements is switched from “dry” to “wet” olivine rheology if the crystallized melt content exceeds some critical value (we take 1 percent). Temperature and composition of accepting elements are recalculated according to the local energy and mass conservation laws.

Extraction of volatiles. We consider two end-member models for the extraction of volatiles. In the first model we assume that CO_2 and HCl are fully extracted from the plume if temperature approaches temperature of the carbonatite solidus⁵⁵. This model gives an upper bound for melt mobility, assuming that melts produced by an infinitely low degree of melting can move out of the plume. In the second model we assume that CO_2 and HCl are fully extracted from both peridotitic and pyroxenitic components only if 1 percent of melting is achieved. This model gives lower boundary for melt mobility, assuming that only 1 percent carbonate-silicate melts can move out of the plume. For both models we assume a concentration of HCl in recycled crust of 137 ppm derived from melt inclusions

in olivine, no HCl in the peridotitic component and minimum conservative estimates of CO₂ content in both recycled crust (900 ppm) and plume peridotite (70 ppm) (see above).

Expected mode of volatiles motion in the lithosphere. Melt from the plume is trapped and crystallizes in the lithosphere, then returns to the mantle as the lithosphere founders. The volatiles extracted by melting of the plume are released as the melt crystallizes because host phases are not stable at the high temperatures at the base of the lithosphere. They migrate upward, then react and are fixed in carbonates or chlorides in the cooler upper part of the lithosphere. Continuous upward migration of high temperature isotherms then decomposes these phases promoting further displacement of the volatile front ahead of the basalt-melting front. According to our model, more than 70% of the mafic magmas generated in the plume crystallized to eclogites and subsided back into the mantle as the densified lithosphere foundered; only less than 30 % were intruded into the crust. However, almost all carbonatite melts traversed the lithosphere and crust because the temperature of the detached blocks was significantly higher than melting temperature of carbonatite. It is therefore likely that a significant part of volatiles released from the plume finally reached the surface promoting explosive eruptions, which are very common in the early stage of Siberian Traps^{11,19} and other LIPs, i.e. Emeishan flood basalts⁵⁶. Note that the volatiles that were initially stored in the minerals of the destructed portions of the lithosphere should be also melted out and could finally reach the surface as well.

Why amount of volatiles released from LIPs could be drastically underestimated? The amount of the released volatiles was previously estimated using only the volume of extruded magmas or magmas intruded into the shallow crust. Disregarded were the magmas that crystallized in the deep crust, and more importantly, much larger volumes of magmas that we propose were involved in the destruction of the lithosphere and never reached the crust, although most of the volatiles extracted from them probably did (see above). Additionally, the recycled crust component of the plume, which contains much

more volatiles than the peridotitic component, was not previously considered in balance calculation.

Estimation of ^{13}C excursion. The ^{13}C isotope change due to the released CO_2 (considered as instantaneous) can be estimated from a simple mass-balance equation³⁸. According to our model, about 172 Ttons of CO_2 is released from the plume – about 70% from recycled crust and rest 30% from peridotite. Assuming $\delta^{13}\text{C} = -12\text{‰}$ for crust-derived CO_2 ref(24) and $\delta^{13}\text{C} = -5\text{‰}$ for peridotite-derived CO_2 , we obtain an average isotopic composition of the plume-released carbon of $\delta^{13}\text{C} = -9.9\text{‰}$. Assuming $\delta^{13}\text{C} = 3.6\text{‰}$ for the initial carbon isotope composition and 300 Ttones of CO_2 (or 82 Ttones of C)²³ for the Late-Permian CO_2 reservoir, we estimate that the magnitude of the carbon isotope excursion was 4.9‰ if all plume-released gases migrated to the surface, and 3.5‰, if only half of them arrived. Both numbers are well within the range of reported values for the Permian-Triassic excursion⁵⁷.

References (continued)

- ³⁴ Stoll, B. *et al.* An automated iridium-strip heater for LA-ICP-MS bulk analysis of geological samples. *Geostandards and Geoanalytical Research* **32**, 5-26 (2008).
- ³⁵ Jarosevich, E. J., Nelen, J. A. & Norberg, J. A. Reference sample fro electron microprobe analysis. *Geostand. Newsl.* **4**, 43-47 (1980).
- ³⁶ Jochum, K. P. *et al.* The preparation and preliminary characterisation of eight geological MPI-DING reference glasses for in-site microanalysis. *Geostandards Newsletter-the Journal of Geostandards and Geoanalysis* **24**, 87-133 (2000).
- ³⁷ Herzberg, C. Identification of Source Lithology in the Hawaiian and Canary Islands: Implications for Origins. *Journal of Petrology* **52**, 113-146 (2011).
- ³⁸ Sobolev, A. V., Hofmann, A. W., Brugmann, G., Batanova, V. G. & Kuzmin, D. V. A quantitative link between recycling and osmium isotopes. *Science* **321**, 536-536, doi:10.1126/science.1158452 (2008).

- 39 Sobolev, A. V., Hofmann, A. W., Sobolev, S. V. & Nikogosian, I. K. An olivine-free mantle source of Hawaiian shield basalts. *Nature* **434**, 590-597, doi:10.1038/nature03411 (2005).
- 40 Beattie, P., Ford, C. & Russell, D. Partition coefficients for olivine[^]melt and orthopyroxene-melt systems. *Contributions to Mineralogy and Petrology* **109**, 212-224. (1991).
- 41 Ryabchikov, I. D. High NiO content in mantle-derived magmas as evidence for material transfer from the Earth's core. *Dokl. Earth Sci.* **389**, 437-439 (2003).
- 42 Humayun, M., Qin, L. P. & Norman, M. D. Geochemical evidence for excess iron in the mantle beneath Hawaii. *Science* **306**, 91-94 (2004).
- 43 Holzapfel, C., Chakraborty, S., Rubie, D. D. & Frost, D. J. Effect of pressure on Fe-Mg, Ni and Mn diffusion in $(\text{Fe}_x\text{Mg}_{1-x})_2\text{SiO}_4$ olivine. *Physics of the Earth and Planetary Interiors* **162**, 186-198 (2007).
- 44 Kelemen, P. B., Hart, S. R. & Bernstein, S. Silica enrichment in the continental upper mantle via melt/rock reaction. *Earth and Planetary Science Letters* **164**, 387-406 (1998).
- 45 Manglik, A. & Christensen, U. R. Effect of lithospheric root on decompression melting in plume-lithosphere interaction models. *Geophysical Journal International* **164**, 259-270, doi:10.1111/j.1365-246X.2005.02811.X (2006).
- 46 Ryabchikov, I. D., Solovova, I. P., Ntaflos, T., Buchl, A. & Tikhonenkov, P. I. Subalkaline picrobasalts and plateau basalts from the Putorana plateau (Siberian continental flood basalt province): II. Melt inclusion chemistry, composition of "primary" magmas and P-T regime at the base of the superplume. *Geochemistry International* **39**, 432-446 (2001).
- 47 Safonov, O.G., Kamenetsky, V.S., & Perchuk, L.L. Links between Carbonatite and Kimberlite Melts in Chloride-Carbonate-Silicate Systems: Experiments and Application to Natural Assemblages. *Journal of Petrology* Advance Access published July 2, 2010, doi:10.1093/petrology/egq034
- 48 Dasgupta, R. & Hirschmann, M. M. The deep carbon cycle and melting in Earth's interior. *Earth and Planetary Science Letters* **298**, 1-13, doi:10.1016/j.epsl.2010.06.039 (2010).

- 49 Sobolev, S. V. & Babeyko, A. Y. What drives orogeny in the Andes? *Geology* **33**, 617-620, doi:10.1130/g21557 (2005).
- 50 Babeyko, A. Y., Sobolev, S. V., Trumbull, R. B., Oncken, O. & Lavier, L. L. Numerical models of crustal scale convection and partial melting beneath the Altiplano-Puna plateau. *Earth and Planetary Science Letters* **199**, 373-388 (2002).
- 51 Poliakov, A. N., Cundall, P. A., Podladchikov, Y. Y. & Lyakhovsky, V. A. in *Flow and creep in the Solar System: observations, modelling and theory.* eds D.B. Stone & S.K. Runcorn) 175–195 (Kluwer Academic Publishers, 1993).
- 52 Katz, R. F., Spiegelman, M. & Langmuir, C. H. A new parameterization of hydrous mantle melting. *Geochemistry Geophysics Geosystems* **4**, 1073, doi:10.1029/2002gc000433 (2003).
- 53 Spandler, C., Yaxley, G., Green, D. H. & Rosenthal, A. Phase relations and melting of anhydrous k-bearing eclogite from 1200 to 1600 degrees C and 3 to 5 GPa. *Journal of Petrology* **49**, 771-795, doi:10.1093/petrology/egm039 (2008).
- 54 Kelemen, P. B., Hirth, G., Shimizu, N., Spiegelman, M. & Dick, H. J. B. A review of melt migration processes in the adiabatically upwelling mantle beneath oceanic spreading ridges. *Philosophical Transactions of the Royal Society a-Mathematical Physical and Engineering Sciences* **355**, 283-318 (1997).
- 55 Dasgupta, R. & Hirschmann, M. M. Effect of variable carbonate concentration on the solidus of mantle peridotite. *American Mineralogist* **92**, 370-379, doi:10.2138/am.2007.2201 (2007).
- 56 Wignall, P.B. et al. Volcanism, mass extinction and carbon isotope fluctuations in the Middle Permian of China. *Science*, **324**, 1179-1182 (2009).
- 57 Retallack, G. J. & Jahren, A. H. Methane release from igneous intrusion of coal during late permian extinction events. *Journal of Geology* **116**, 1-20, doi:10.1086/524120 (2008).

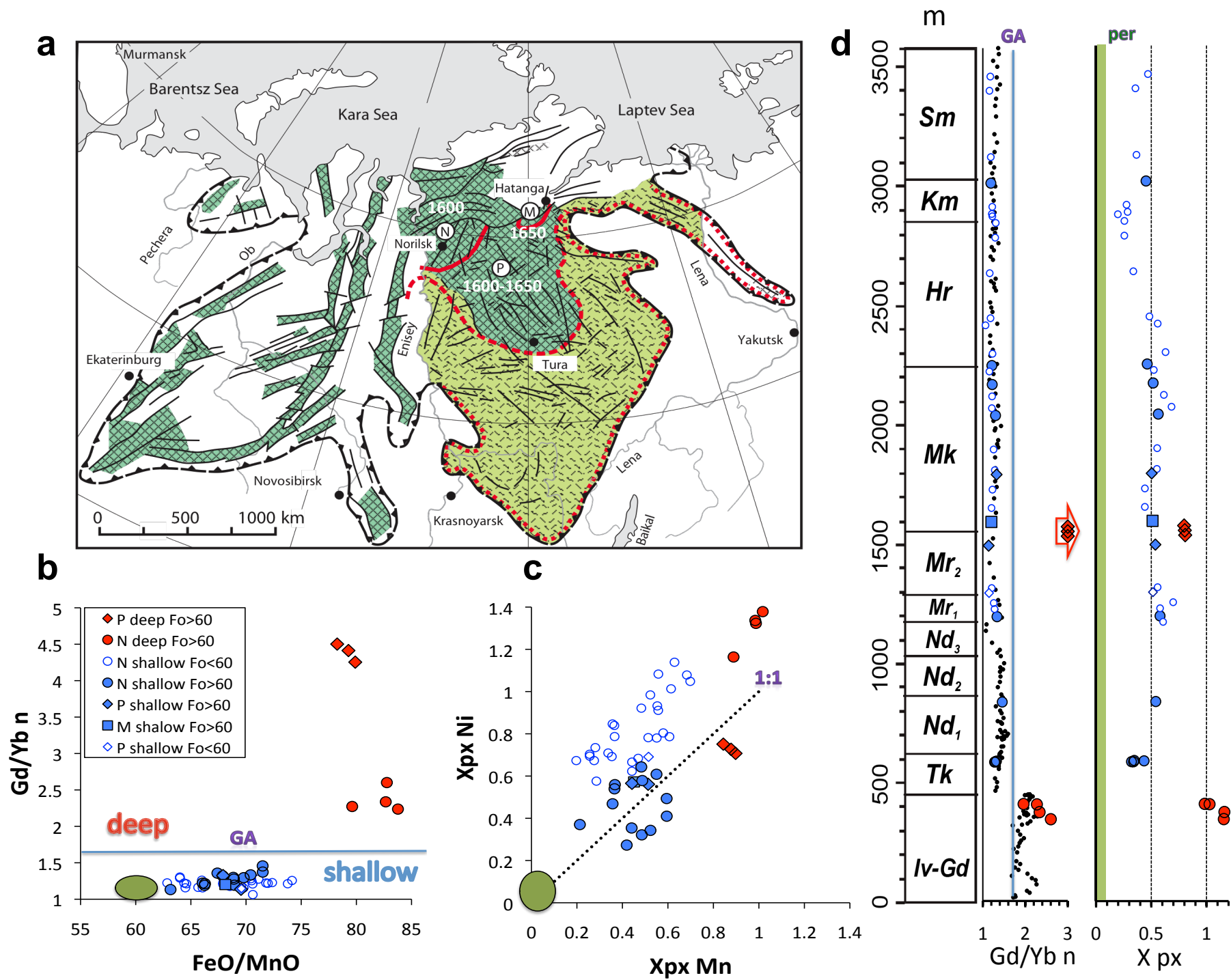


Fig. 1

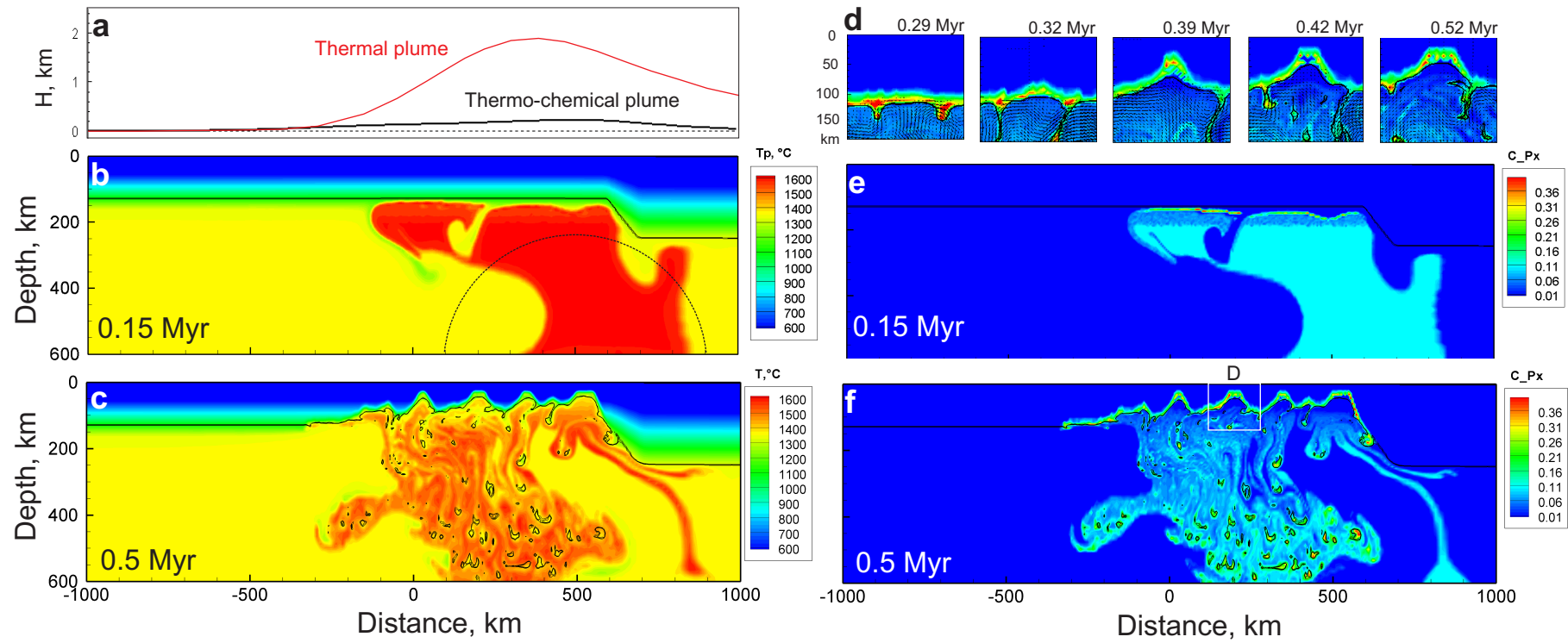


Fig. 2

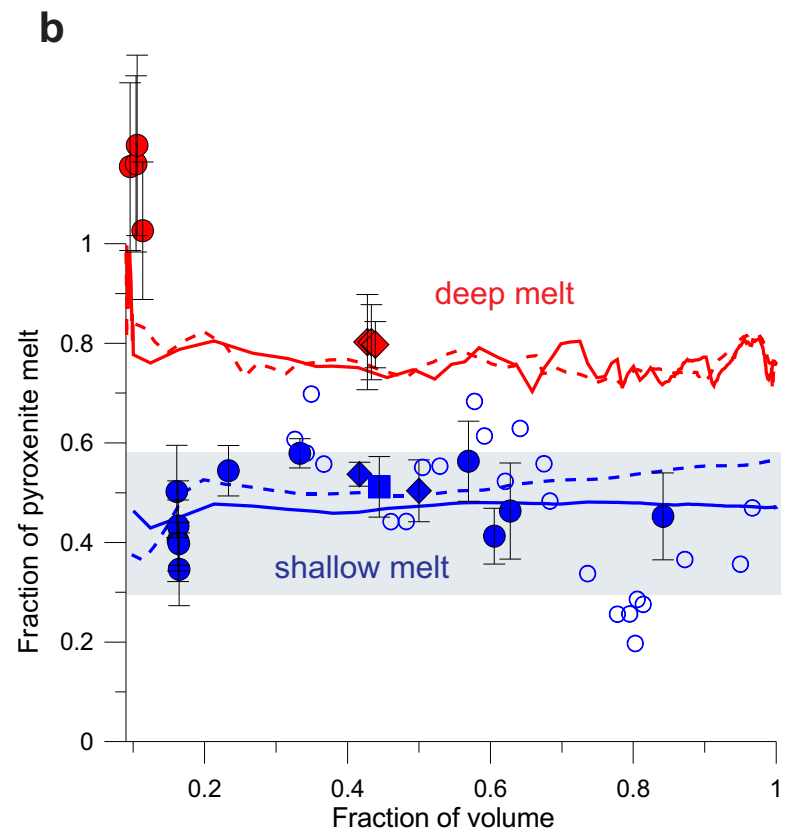
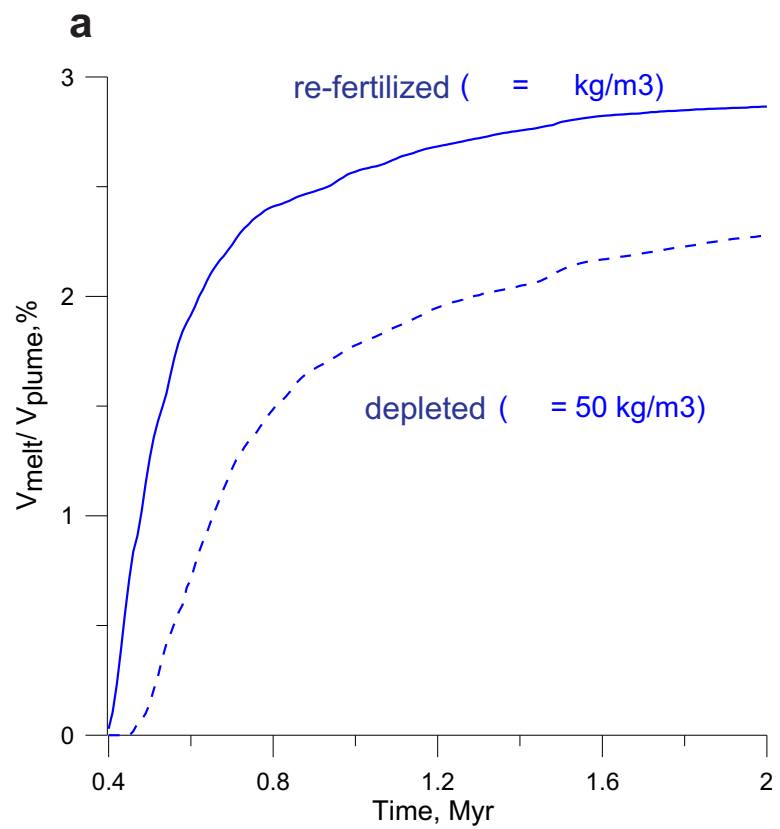


Fig. 3

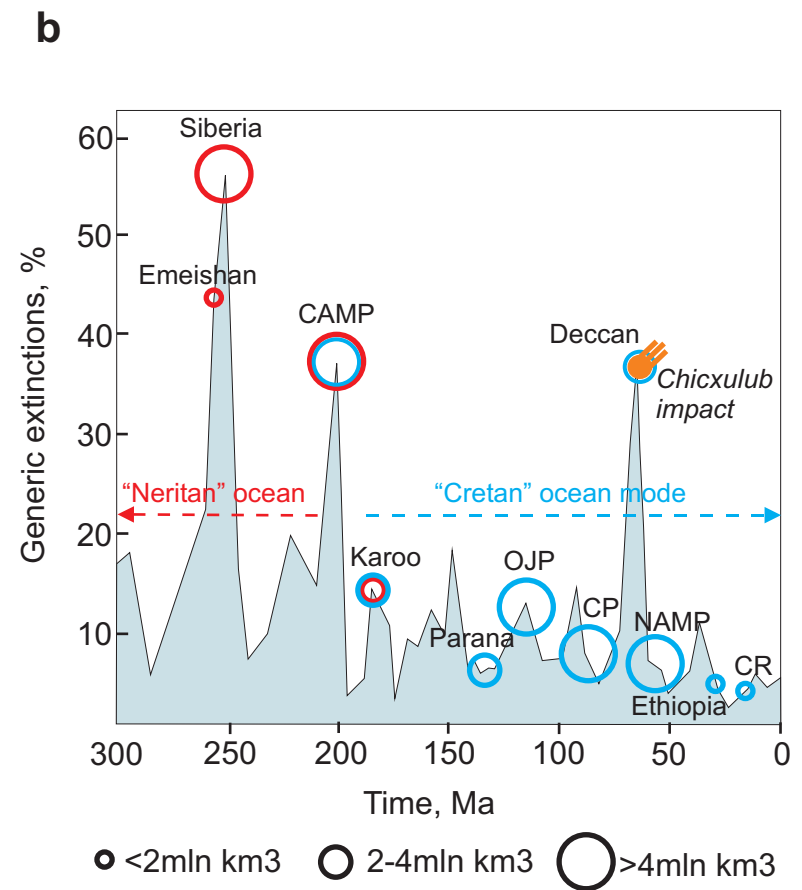
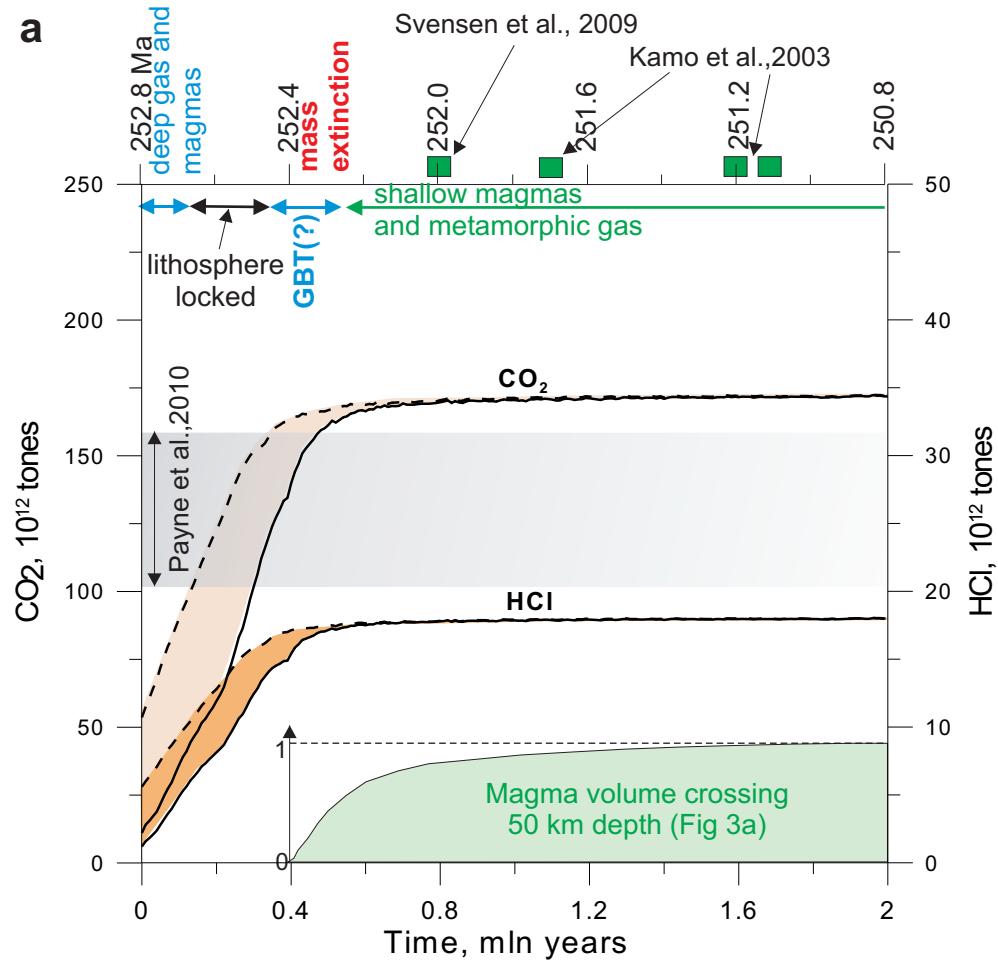


Fig. 4

SUPPLEMENTARY INFORMATION

Samples description

Studied samples are olivine phyric, olivine-plagioclase phyric or aphyric basalts and rarely picrites from outcrops or drill core of lava flows (most samples), and outcrops of dykes (few samples) see Table S1. They contain visually fresh olivine phenocrysts, microphenocrysts or olivine-pyroxene intergrowths and were carefully selected from lavas from Norilsk area, Putorana plateau and Maymecha-Kotuy province.

Norilsk area. We studied samples from most lava units of the Norilsk section, covering most parts of the region¹⁻⁴. Samples were carefully located relative to the lower boundaries of the units and were placed within the integrated lava section of Siberian traps using this information and absolute positions of unit boundaries after Fedorenko et al, 1996 ref(1). Abbreviations at Fig. 1D indicate the following lava suites of the Norilsk area placed in the order of decreasing age: Iv-Ivinskaya, Gd-Gudchikhinskaya, Tk-Tuklonskaya, Nd-Nadezhdinskaya, Mr-Morangovskaya, Mk-Mukulaevskaya, Hr-Haerlakhskaya, Km-Kumginskaya, Sm-Samoedskaya. $(Gd/Yb)_n$ indicates the element ratio normalized to the primitive mantle composition of Hofmann, 1988 ref(5). We also studied olivine phyric basaltic dykes (samples 22-12 and 22-6), cutting the upper Mukulaevskaya suite and thus representing any of upper units from Hr to Sm.

Putorana plateau. Studied samples came from collection of V. Nesterenko⁶⁻⁹ and Y. Vasiliev (picrites of Ayan river)¹⁰. We estimated approximate positions of studied samples in the integrated lava section (Fig 1D) using data reported in ref(1, 6).

Maymecha-Kotuy province. Most lavas of this province are highly alkaline^{11, 12} and are not discussed in this paper. Here we report olivine compositions from only one sample, which represents the major type of voluminous tholeiitic lavas from the Maymecha-Kotuy province¹³. It is similar in composition to the predominant type of Norilsk and Putorana basalts and is placed in the integrated lava section (Fig 1D) using the data of ref(1).

SUPPLEMENTARY INFORMATION

Olivine compositions

Magmas originated from mantle peridotite or reaction pyroxenite should crystallize magnesian olivine at low pressures^{14,15}. The minimum forsterite component is expected for olivine in equilibrium with melt originated from the pure pyroxenitic source. Sobolev et al (2009) ref(3) estimated the composition of such an olivine to be in the range of Fo84-86 similar to the most magnesian composition of actual olivine from lavas of Gudchikhinkaya formation (up to Fo 83.5, ref(3, 14)). This suggests minimal fractionation of these lavas. The subalkaline picrites from Ayan River on the Putorana plateau have also high-Mg olivine (up to Fo 90, see Fig S1) and thus a low degree of fractionation. The shallow-derived Siberian lavas (no garnet in the source) underwent more crystal fractionation and highly magnesian olivine is exceptionally rare in these lavas. Here we report olivine with up to Fo79 in upper, most voluminous volcanic formations of Norilsk area and corresponding lava suites at Maymecha-Kotuy and Putorana regions (see Fig S1). This value is more magnesian than previously reported in these suites. Figure S1 compares the compositions of the most magnesian olivines reported in this paper with compositions of olivine expected to crystallize from peridotite-derived magmas^{14, 15}. For the same Fo content, all Siberian olivines are significantly higher in Ni and lower in Mn (seen also in higher FeO/MnO ratio) than olivine from peridotite derived magmas. Crystallization of large amounts of early clinopyroxene could potentially create a similar affect in coexisting olivine. This is demonstrated by compositional trend of olivine from sample CY-315 from Tuklonskaya formation (Fig S1). This olivine has lowest Ni of the all Siberian samples and defines the flattest trend in Fo-NiO space. In this olivine CaO decreases rapidly and FeO/MnO increases with decreasing Fo. Thus for this lava we cannot exclude the possibility that the primary high-Mg melt was derived from a peridotite- dominated source. However, the CaO contents of olivine from other samples do not support this interpretation (see Fig S1c). Instead, we suggest that high Ni and low Mn in Siberian olivines imply a large fraction of non peridotitic lithology in their source^{14,15}. We note that FeO/MnO ratio of olivine does not change significantly during shallow fractional crystallization as indicated by the trends on Figure S1d. This supports the use of this ratio for estimating amount of pyroxenitic

SUPPLEMENTARY INFORMATION

component for highly evolved low magnesian olivine. The most magnesian olivine reported here (Fo79) comes from the most voluminous traps lavas but it is still much less magnesian than expected for their primary melts. This may suggest that an early stage of their fractionation took place at deep magma chambers, perhaps at 40-50 km depth close to the level of their origin predicted by model.

Calculation of density

Apart from temperature, pressure and initial composition, the densities of all materials are assumed to be affected by variable content of melt, crystallized melt or melt extraction. All these effects are linearized and are considered in Boussinesq approximation. Density of material *i* is

$$\rho_i = \rho_i^0(P, T) (1 - a_i^{pr} \cdot X_{pr} + a_i^{px} \cdot X_{px} + a_i^{epx} \cdot X_{epx} + a_i^{epr} \cdot X_{epr} + a_i^{mpx} \cdot X_{mpx} + a_i^{mpr} \cdot X_{mpr}) \quad (S1)$$

Where $\rho_i^0(p, T)$ is density of pure non molten *i*-th material, X_{pr} is concentration of extracted peridotitic melt, X_{px} is concentration of the pyroxenitic component, X_{epx} is concentration of crystallized melt derived from the pyroxenitic component, X_{epr} is concentration of crystallized melt derived from the peridotitic component, X_{mpx} is concentration of melt derived from the pyroxenitic component, X_{mpr} is concentration of melt derived from the peridotitic component. All concentrations are volume concentrations. Multipliers of concentrations are constants depending on material and pressure. Parameters related to melt a_i^{mpx}, a_i^{mpr} were assumed to be -0.1 for all materials. Values for “a” parameters related to crystallized melt and pyroxenitic component in mantle materials (mantle lithosphere, asthenosphere and plume) were estimated calculating rock densities for different pressure and temperature from bulk chemical compositions of pyroxenite-derived³ and peridotite-derived basalts¹⁶ using a thermodynamic modeling approach¹⁷. For density effect of melt extraction from peridotite (depletion) we use data¹⁸. All these parameters were found to be close to 0.05 (0.045-0.055) in the eclogite stability field. For

SUPPLEMENTARY INFORMATION

simplicity, we assume them to be equal to 0.05 in the eclogite stability field (here at depth > 55 km). Change of density due to gabbro-eclogite transformation¹⁷ is considered by linearly decreasing “a” parameters from 0.05 at depth of 55 km to -0.05 at depth of 40 km.

With the accepted values of parameters, the buoyancy of the thermo-chemical plume with an excess temperature of 250 °C ($T_p=1600^\circ\text{C}$) and an eclogite content of 15 % is only 10% of the buoyancy of the purely thermal plume with the same temperature.

Model setup

The setup and boundary conditions for our preferred model are presented in Fig. S2. We assume that the plume head arrives at the base of the cratonic root at model time 0. The left model boundary is open for inwards- and outwards flow of material, while the right boundary and bottom are closed, to avoid instabilities. We use a non-uniform grid to better resolve the central part of the model. Finite element size is 5X5 km in the best-resolved part of the model. Tests show no significant influence on model results of mesh coarsening out of that region. Plume temperature for the preferred model is $T_p=1600^\circ\text{C}$ and the content of recycled oceanic crust (eclogite) is 15 wt%.

Evolution in time of temperature and pyroxenite content are shown in Fig. S3.

Model sensitivity and choice of the preferred model

The intensity of lithospheric destruction and melt production depend on (1) the initial thickness and degree of depletion of the lithosphere (Fig. S4), (2) plume temperature, and volume (Fig. S5), and (3) content of the recycled crust in the plume (Fig. S6).

Our preferred model is constrained by the petrological data, i.e. a plume head potential temperature of 1600°C , 15 wt% of recycled crust, and an initial thickness of depleted lithosphere of 130 km. A plume head radius of 400 km was chosen arbitrarily. With the fixed initial thickness of the lithosphere, a lower

SUPPLEMENTARY INFORMATION

plume potential temperature (1500-1550°C instead of 1600°C in preferred model), or a smaller plume (200-300 km radius instead of 400 km) would result in much less extensive lithospheric delamination and lower melt production (Fig. S5). A content of recycled crust significantly higher than 15 wt% makes the plume negatively buoyant (at plume potential temperature of 1600°C), while a lower content results in large pre-magmatic uplift (Fig. S6).

We prefer a model of re-fertilized mantle lithosphere because the lithosphere of Siberian Craton experienced multiple interactions with mantle plumes before the emplacement of Siberian Traps, as evidenced by multiple phases of kimberlite magmatism and synchronous flood basalts^{19,20}. Choosing depleted lithosphere with two-times larger density deficit does not significantly change the results (Fig. 3a main text, dashed curve and (Fig. S4)). However, further rise of the average degree of depletion and density deficit, to 60 and 70 kg/m³, significantly impedes lithospheric destruction (Fig. S4).

Supplementary References

- 1 Fedorenko, V. A. *et al.* Petrogenesis of the flood-basalt sequence at Noril'sk, North Central Siberia. *International Geology Review* **38**, 99-135 (1996).
- 2 Krivolutskaya, N. & Rudakova, A. Structure and Geochemical Characteristics of Trap Rocks from the Noril'sk Trough, Northwestern Siberian Craton. *Geochemistry International* **47**, 675-698, doi:10.1134/S0016702909070015 (2009).
- 3 Sobolev, A. V., Krivolutskaya, N. A. & Kuzmin, D. V. Petrology of the parental melts and mantle sources of Siberian trap magmatism. *Petrology* **17**, 253-286, doi:10.1134/s0869591109030047 (2009).
- 4 Krivolutskaya, N. A., Sobolev, A. V., Mikhailiov, V. N. & Svirskaya, N. M. New data concerning the high-Mg rocks of the Siberian trap formation in the Noril'sk region. *Geochimica Et Cosmochimica Acta* **71**, A525-A525 (2007).
- 5 Hofmann, A. W. Chemical differentiation of the Earth: the relationship between mantle, continental crust, and oceanic crust. *Earth Planet. Sci. Lett.* **90**, 297-314 (1988).

SUPPLEMENTARY INFORMATION

- 6 Nesterenko, G. V., Tikhonenkov, P. I. & Kolesov, G. M. RARE-EARTH ELEMENTS
IN PLATEAU-BASALT OF THE SIBERIAN PLATFORM. *Geokhimiya*, 823-834
(1990).
- 7 Nesterenko, G. V., Tikhonenkov, P. I. & Romashova, T. V. BASALTS OF PUTORANA
PLATEAU. *Geokhimiya*, 1419-1425 (1991).
- 8 Sharma, M., Basu, A. R. & Nesterenko, G. V. ND-SR ISOTOPES, PETROCHEMISTRY,
AND ORIGIN OF THE SIBERIAN FLOOD BASALTS, USSR. *Geochimica Et
Cosmochimica Acta* **55**, 1183-1192 (1991).
- 9 Sharma, M., Basu, A. R. & Nesterenko, G. V. TEMPORAL SR-ISOTOPIC, ND-
ISOTOPIC AND PB-ISOTOPIC VARIATIONS IN THE SIBERIAN FLOOD BASALTS -
IMPLICATIONS FOR THE PLUME-SOURCE CHARACTERISTICS. *Earth and
Planetary Science Letters* **113**, 365-381 (1992).
- 10 Vasilev, Y. R. Plagioclase bearing picrites of Ayan river. *Russian Geology and
Geophysics*, 68-75 (1988).
- 11 Vasiliev, Y. R. & Zolotukhin, V. V. The Maimecha-Kotui alkaline-ultramafic
province of the northern Siberian Platform, Russia. *Episodes* **18**, 155-164 (1995).
- 12 Arndt, N., Chauvel, C., Czamanske, G. & Fedorenko, V. Two mantle sources, two
plumbing systems: tholeiitic and alkaline magmatism of the Maymecha River
basin, Siberian flood volcanic province. *Contributions to Mineralogy and
Petrology* **133**, 297-313 (1998).
- 13 Vasilev, Y. R. Low potassium basalts of Maimecha-Kotuy province and their likely
geodynamic setting. *Doklady Akademii Nauk* **366**, 507-510 (1999).
- 14 Sobolev, A. V. *et al.* The amount of recycled crust in sources of mantle-derived
melts. *Science* **316**, 412-417, doi:10.1126/science.1138113 (2007).
- 15 Herzberg, C. Identification of Source Lithology in the Hawaiian and Canary
Islands: Implications for Origins. *Journal of Petrology* **52**, 113-146 (2011).
- 16 Walter, M. J. Melting of garnet peridotite and the origin of komatiite and depleted
lithosphere. *Journal of Petrology* **39**, 29-60 (1998).
- 17 Sobolev, S. V. & Babeyko, A. Y. MODELING OF MINERALOGICAL COMPOSITION,
DENSITY AND ELASTIC-WAVE VELOCITIES IN ANHYDROUS MAGMATIC ROCKS.
Surveys in Geophysics **15**, 515-544 (1994).
- 18 Schutt, D. L. & Leshner, C. E. Effects of melt depletion on the density and seismic
velocity of garnet and spinel lherzolite. *Journal of Geophysical Research-Solid
Earth* **111**, B05401, doi: 10.1029/2003jb002950 (2006).
- 19 Griffin, W. L. *et al.* The Siberian lithosphere traverse: mantle terranes and the
assembly of the Siberian Craton. *Tectonophysics* **310**, 1-35 (1999).

SUPPLEMENTARY INFORMATION

- 20 Kuzmin, M. I., Yarmolyuk, V. V. & Kravchinsky, V. A. Phanerozoic hot spot traces and paleogeographic reconstructions of the Siberian continent based on interaction with the African large low shear velocity province. *Earth-Science Reviews* **102**, 29-59, doi:10.1016/j.earscirev.2010.06.004 (2010).
- 21 Gleason, G.C. & Tullis, J. A flow law for dislocation creep of quartz aggregates determined with the molten salt cell. *Tectonophysics* **247**, 1-23 (1995).
- 22 Rybacki, E. & Dresen, G. Dislocation and diffusion creep of synthetic anorthite aggregates. *J. Geophys. Res.* **105**, 26017-26036 (2000).
- 23 Hirth, G. & Kohlstedt, D. L. in *In Inside the Subduction Factory* Vol. 138 (ed J. Eiler) 83-105 (American Geophysical Union 2003).

SUPPLEMENTARY INFORMATION

Table S1. Studied samples and olivine.

Sample	Group	Region	Unit	Ref	Type	Thick m	N1	Max Fo	N2	Avg Fo (3)	Xpx Ni	S.e	Xpx Mn	S.e	Xpx	S.e	FeO/MnO	Gd/Yb n
SU-50	Deep	Nor	Gd	S3	lava	345	128	81.32	75	79.71	1.32	0.01	0.99	0.00	1.15	0.17	82.8	2.60
4270/13	Deep	Nor	Gd	S3	lava	375	47	80.47	33	79.18	1.34	0.01	0.98	0.00	1.16	0.18	82.7	2.34
86-77	Deep	Nor	Gd	new	lava	380	52	80.69	7	79.12	1.38	0.03	1.02	0.01	1.20	0.18	83.8	2.24
XS-51/130	Deep	Nor	Gd	S3	lava	408	120	83.32	85	81.51	1.16	0.00	0.89	0.00	1.03	0.14	79.6	2.27
991a	Deep	Put	Ay	new	lava	1540	98	90.04	44	87.85	0.71	0.01	0.90	0.01	0.80	0.10	79.9	4.25
991b	Deep	Put	Ay	new	lava	1560	103	89.45	42	87.26	0.73	0.01	0.88	0.01	0.80	0.08	79.3	4.41
81-133	Deep	Put	Ay	new	lava	1580	100	88.39	73	86.59	0.75	0.00	0.84	0.00	0.80	0.05	78.3	4.50
86-86	Sh (Fo>60)	Nor	Tk	new	lava	580	9	71.93	9	70.87	0.41	0.01	0.59	0.01	0.50	0.09	71.5	1.37
SU31	Sh (Fo>60)	Nor	Tk	S3	lava	586	75	76.66	14	74.92	0.32	0.01	0.49	0.01	0.40	0.08	68.9	1.28
SU33	Sh (Fo>60)	Nor	Tk	S3	lava	587	8	73.57	8	73.02	0.34	0.01	0.52	0.01	0.43	0.09	69.8	1.30
SU36	Sh (Fo>60)	Nor	Tk	new	lava	590	16	76.66	7	74.22	0.35	0.01	0.44	0.01	0.40	0.04	67.9	1.32
CY-315	Sh (Fo>60)	Nor	Tk	new	lava	592	62	77.28	54	75.59	0.27	0.00	0.42	0.01	0.35	0.07	67.4	1.36
530/12	Sh (Fo>60)	Nor	Nd	S3	lava	840	17	79.41	1	79.41	0.49		0.59		0.54	0.05	71.5	1.46
140-1	Sh (Fo>60)	Nor	Mr	new	lava	1200	34	67.96	2	67.74	0.61	0.04	0.55	0.08	0.58	0.03	70.4	1.33
4002-14	Sh (Fo>60)	Nor	Mk	new	lava	2049	36	62.78	1	62.78	0.64		0.48		0.56	0.08	68.8	1.30
47-1	Sh (Fo>60)	Nor	Mk	new	lava	2180	85	72.78	1	72.78	0.47		0.36		0.41	0.06	66.1	1.22
4002-18	Sh (Fo>60)	Nor	Hr	new	lava	2260	68	68.99	23	66.99	0.56	0.00	0.37	0.00	0.46	0.10	66.3	1.21
63	Sh (Fo>60)	Nor	Sm	new	lava	3030	89	73.09	2	72.38	0.54	0.02	0.37	0.02	0.45	0.09	66.2	1.19
85-63	Sh (Fo>60)	Put	Ay	new	lava	1500	57	71.94	3	70.29	0.56	0.03	0.51	0.00	0.54	0.02	69.5	1.14
83-50	Sh (Fo>60)	Put	Ho	new	lava	1800	39	69.26	2	68.83	0.57	0.03	0.44	0.01	0.50	0.06	67.9	1.32
1934-2	Sh (Fo>60)	M-K	On	new	lava	1600	115	77.33	5	75.61	0.57	0.03	0.45	0.02	0.51	0.06	68.1	1.20
141-7	Sh (Fo<60)	Nor	Nd	new	lava	1175	48	48.65	28	46.54	0.79	0.01	0.61	0.01	0.61		71.8	1.22
126-3	Sh (Fo<60)	Nor	Mr	new	lava	1232	67	52.82	6	50.77	0.80	0.02	0.58	0.03	0.58		71.1	1.28
126-4	Sh (Fo<60)	Nor	Mr	new	lava	1258	48	52.19	6	50.70	1.05	0.02	0.70	0.01	0.70		74.2	1.26
126-7	Sh (Fo<60)	Nor	Mr	new	lava	1321	36	50.44	12	49.06	0.91	0.01	0.56	0.01	0.56		70.6	1.21
4002-2	Sh (Fo<60)	Nor	Mk	new	lava	1659	59	56.25	1	56.25	0.62		0.44		0.44		67.9	1.20
4002-5	Sh (Fo<60)	Nor	Mk	new	lava	1736	69	57.59	5	56.88	0.67	0.02	0.44	0.03	0.44		67.9	1.23
4002-7	Sh (Fo<60)	Nor	Mk	new	lava	1818	52	59.60	3	58.74	0.78	0.02	0.55	0.01	0.55		70.4	1.28
4002-11	Sh (Fo<60)	Nor	Mk	new	lava	1906	73	54.00	11	52.17	0.93	0.02	0.55	0.01	0.55		70.5	1.25
46-1	Sh (Fo<60)	Nor	Mk	new	lava	2080	45	49.50	45	48.33	1.08	0.01	0.68	0.01	0.68		73.8	1.21
19-1	Sh (Fo<60)	Nor	Mk	new	lava	2130	12	48.75	7	46.70	1.01	0.04	0.61	0.02	0.61		72.0	1.22
136-13	Sh (Fo<60)	Nor	Mk	new	lava	2235	51	49.37	36	47.30	0.98	0.01	0.52	0.01	0.52		69.8	1.15
4002-19	Sh (Fo<60)	Nor	Hr	new	lava	2310	60	47.30	60	46.16	1.14	0.01	0.63	0.00	0.63		72.4	1.23
137-2	Sh (Fo<60)	Nor	Hr	new	lava	2430	27	51.33	9	50.02	1.08	0.02	0.56	0.01	0.56		70.6	1.06
61-3	Sh (Fo<60)	Nor	Hr	new	lava	2460	12	47.07	12	45.85	0.92	0.02	0.48	0.01	0.48		68.8	1.18
115-1	Sh (Fo<60)	Nor	Hr	new	lava	2650	111	59.01	1	59.01	0.71		0.34		0.34		65.7	1.16
115-9	Sh (Fo<60)	Nor	Hr	new	lava	2800	75	53.44	6	51.21	0.70	0.01	0.26	0.02	0.26		64.0	1.29
62	Sh (Fo<60)	Nor	Km	new	lava	2862	6	46.53	1	46.53	0.69		0.26		0.26		64.0	1.30
62-1	Sh (Fo<60)	Nor	Km	new	lava	2890	37	47.53	12	45.78	0.67	0.01	0.20	0.01	0.20		62.8	1.22
119-1	Sh (Fo<60)	Nor	Km	new	lava	2900	48	56.31	1	56.31	0.58		0.29		0.29		64.6	1.21
137-11	Sh (Fo<60)	Nor	Km	new	lava	2930	18	53.50	2	52.55	0.67	0.02	0.28	0.08	0.28		64.4	1.22
125-4	Sh (Fo<60)	Nor	Sm	new	lava	3140	74	58.55	12	57.24	0.79	0.01	0.37	0.01	0.37		66.3	1.19
65-4	Sh (Fo<60)	Nor	Sm	new	lava	3420	83	51.51	8	49.82	0.85	0.02	0.36	0.01	0.36		66.1	1.16
65-5	Sh (Fo<60)	Nor	Sm	new	lava	3480	48	55.36	1	55.36	0.68		0.47		0.47		68.5	1.18
81-134	Sh (Fo<60)	Put	Ay	new	lava	1300	26	59.80	1	59.80	0.69		0.51		0.51		69.6	1.15
22-6	Sh (Fo<60)	Nor	Hr-Sm	new	dyke	-	71	75.27	15	73.67	0.58	0.01	0.49	0.01	0.53	0.05	68.9	1.19
22-12	Sh (Fo<60)	Nor	Hr-Sm	new	dyke	-	51	78.52	28	76.64	0.37	0.00	0.21	0.01	0.29	0.08	63.2	1.13
12-1	Sh (Fo<60)	Nor	Hr-Sm	new	dyke	-	56	48.62	12	46.72	0.69	0.02	0.35	0.01	0.35		66.0	1.26
39-3	Sh (Fo<60)	Nor	Hr-Sm	new	dyke	-	98	54.21	87	52.46	0.84	0.00	0.36	0.00	0.36		66.2	1.22
125-5	Sh (Fo<60)	Nor	Hr-Sm	new	dyke	-	50	48.12	24	45.80	0.78	0.01	0.51	0.01	0.51		69.6	1.18
120	Sh (Fo<60)	Nor	Hr-Sm	new	dyke	-	75	61.16	34	59.49	0.73	0.00	0.28	0.00	0.28		64.5	1.16

Table S1 notes. Group: deep (high Gd/Ybn>1.6 =garnet signature), Sh- shallow (low Gd/Ybn< 1.6 = no garnet in the source), Fo- maximum amount of Forsterite content in olivine in the sample. Region: Nor-Norilsk, Put-Putorana plateau, M-K- Maymecha-Kotuy province. Unit: (Norilsk region Gd-Gudchikhinskaya, Tk-Tuklonskaya, Nd-Nadezhdinskaya, Mr-Morangovskaya, Mk-Mukulaevskaya, Hr-Haerlakhsakaya, Km-Kumginskaya, Sm-Samoedskaya; Putorana plateau Ay-Ayanskaya, Ho-Honumanskaya; Maymecha-Kotuy province On- Onkuchakskaya. Ref: references. Type: lavas or dykes. Thick: thickness in meters. N1: Total amount of olivine grains analyzed. Max Fo : composition of most magnesian olivine. N2: amount of olivine grains having composition within maximum 3 mol% Fo. Avg Fo (3)- average of most magnesian olivine grains having composition within maximum 3 mol% Fo. Xpx Ni and Xpx Mn- proportion of pyroxenite derived melt calculated from Ni excess and Mn deficiency correspondingly in average most magnesian olivine. Xpx-accepted proportion of pyroxenite derived melt (see text). S.e.- standard error of mean. FeO/MnO- corresponding ratio for the average most magnesian olivine. Gd/Ybn- normalized to primitive mantle ⁵ ratio of bulk rock.

SUPPLEMENTARY INFORMATION

Table S2. Model parameters.

Parameter	Upper crust	Lower crust	Depleted mantle lithosphere	Asthenosphere / plume
Density, [kg/m ³]	2750	2950	3330- $\Delta\rho_{\text{depl}}$	3330
Thermal expansion, [K ⁻¹]	3.7·10 ⁻⁵	2.7·10 ⁻⁵	3.3·10 ⁻⁵	3.3·10 ⁻⁵
Elastic moduli, K, G, [GPa]	55, 36	63, 40	122, 74	122, 74
Heat capacity, [J/kg/K]	1200	1200	1200	1200
Heat conductivity, [W/K/m]	2.5	2.5	3.3	3.3
Heat productivity, [W/m ³]	1.3	0.2	0	0
Initial friction angle, [degree]	30	30	30	30
Initial cohesion, [MPa]	20	20	20	20
Diffusion creep, log(A), [Pa ⁻ⁿ s ⁻¹]	-	-	-10.59	-10.59
Diffusion creep activation energy, [kJ/mol]	-	-	300	300
Grain size[mm];Grain size exponent	-	-	1.0;2.5	1.0;2.5
Dislocation creep, log(A), [Pa ⁻ⁿ s ⁻¹]	-28.0	-15.4	-15.2	-14.7/-14.3
Dislocation creep activation energy, [kJ/mol]	223	356	530	515
Power law exponent	4.0	3.0	3.5	3.5

Table S2 notes. Sources for dislocation creep laws: upper crust – quartzite²¹; lower crust – wet plagioclase²²; depleted mantle lithosphere – dry peridotite²³, asthenosphere – wet peridotite with 1000 Ppm H₂O (asthenosphere) and 2000 Ppm H₂O (plume)²³.

Table S3. Compositions of olivine and host lavas. (Excel file).

SUPPLEMENTARY INFORMATION

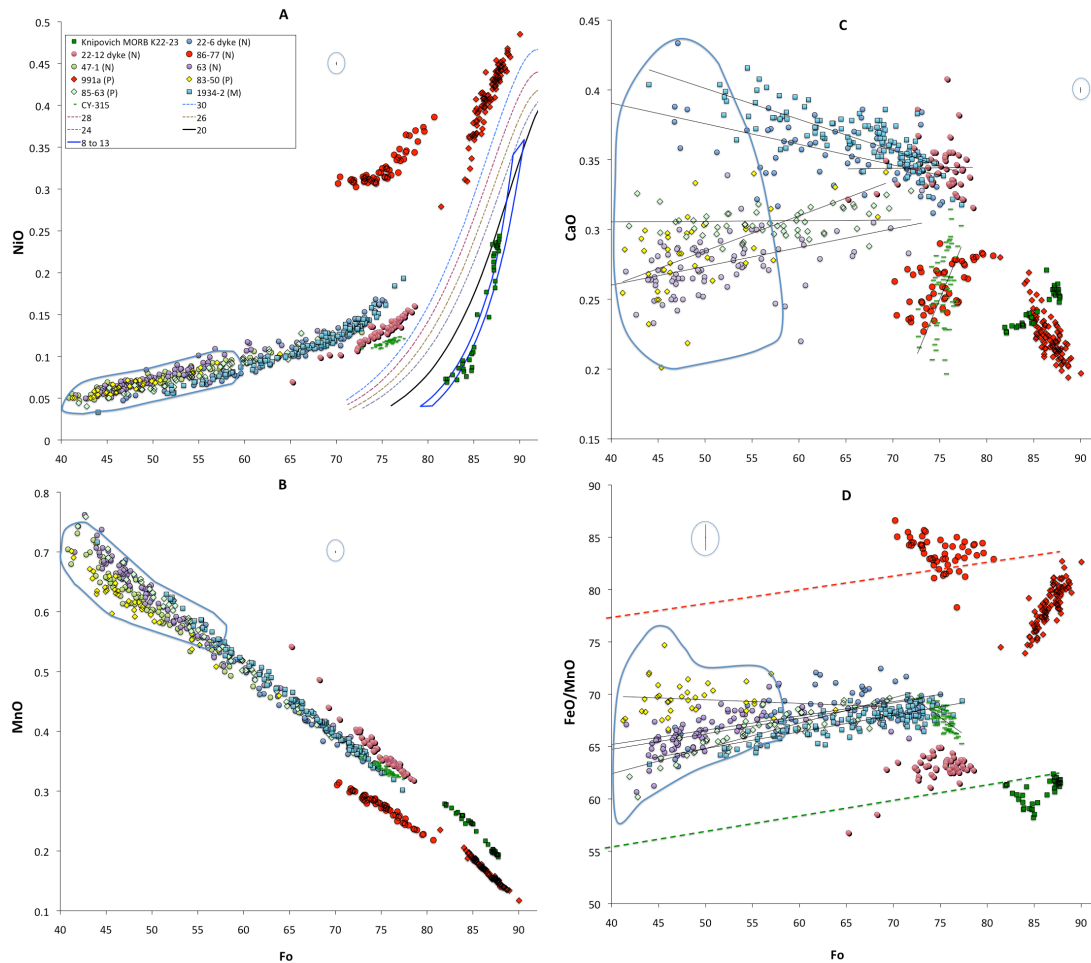


Fig. S1. Compositions of representative Siberian trap olivine, compared with olivine from peridotite derived melts.

A. Numbered lines and field are compositions of olivine crystallized from peridotite derived melt with initial MgO content indicated by corresponding number(15). Blue field outline compositions of low magnesian olivines (Fo<60) from Siberian traps (Table S4). Knipovich MORB K22-23- stands for olivine compositions from Knipovich ridge MORB sample with almost zero content of pyroxenitic component in the melt (14).

C. Solid black lines indicate linear regression lines for the olivine of different samples. Other symbols are as on Fig S1A.

D. Dashed red and green lines are suggested boundaries for FeO/MnO ratios of end-member olivines crystallized from pyroxenite and peridotite derived melts respectively. Slope of these lines constrained to be parallel to the dominant slope of trend lines. Other symbols are as on Fig S1A,B.

Error bars outlined by the blue circle are 2-standard deviations estimated from repeated analyses of olivine standard.

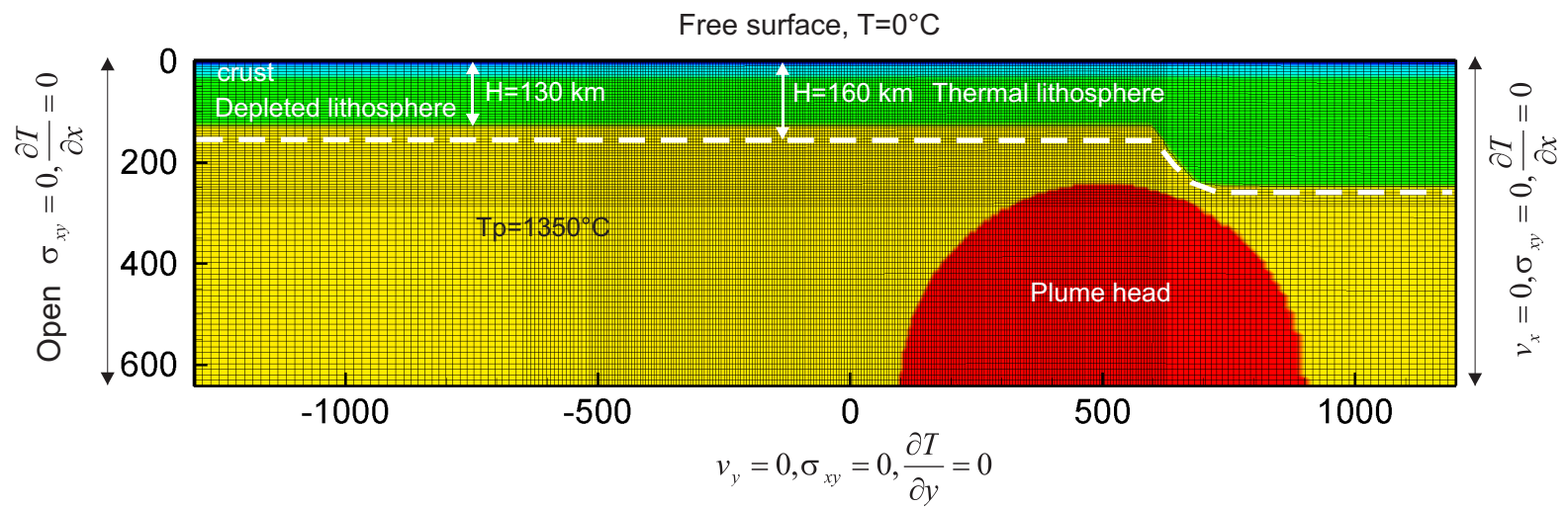


Fig. S2. Initial and boundary conditions for the preferred model

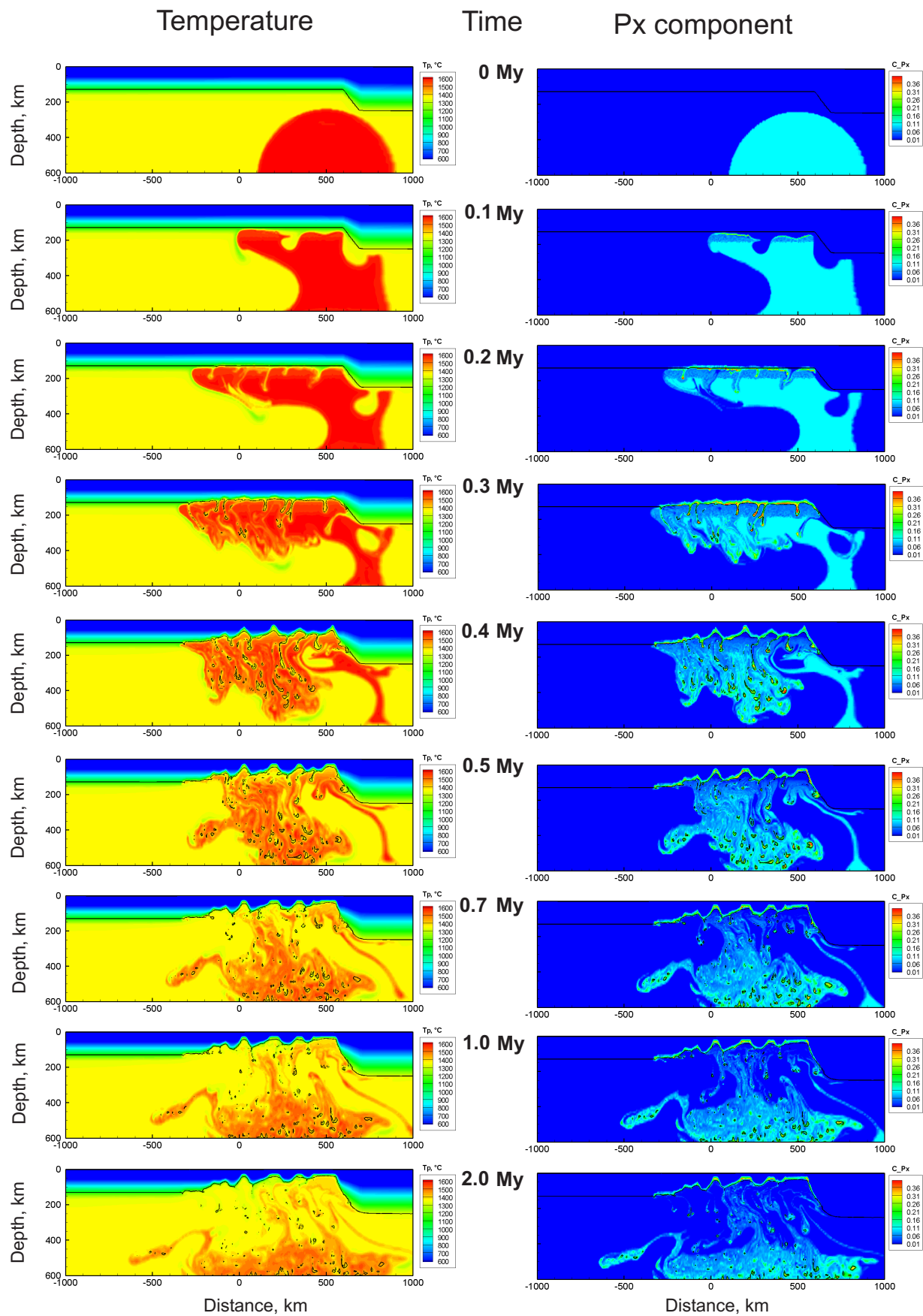


Fig. S3. Evolution of the temperature distribution (left column) and of distribution of the pyroxenite component in the plume or in the crystallized melt (right column)

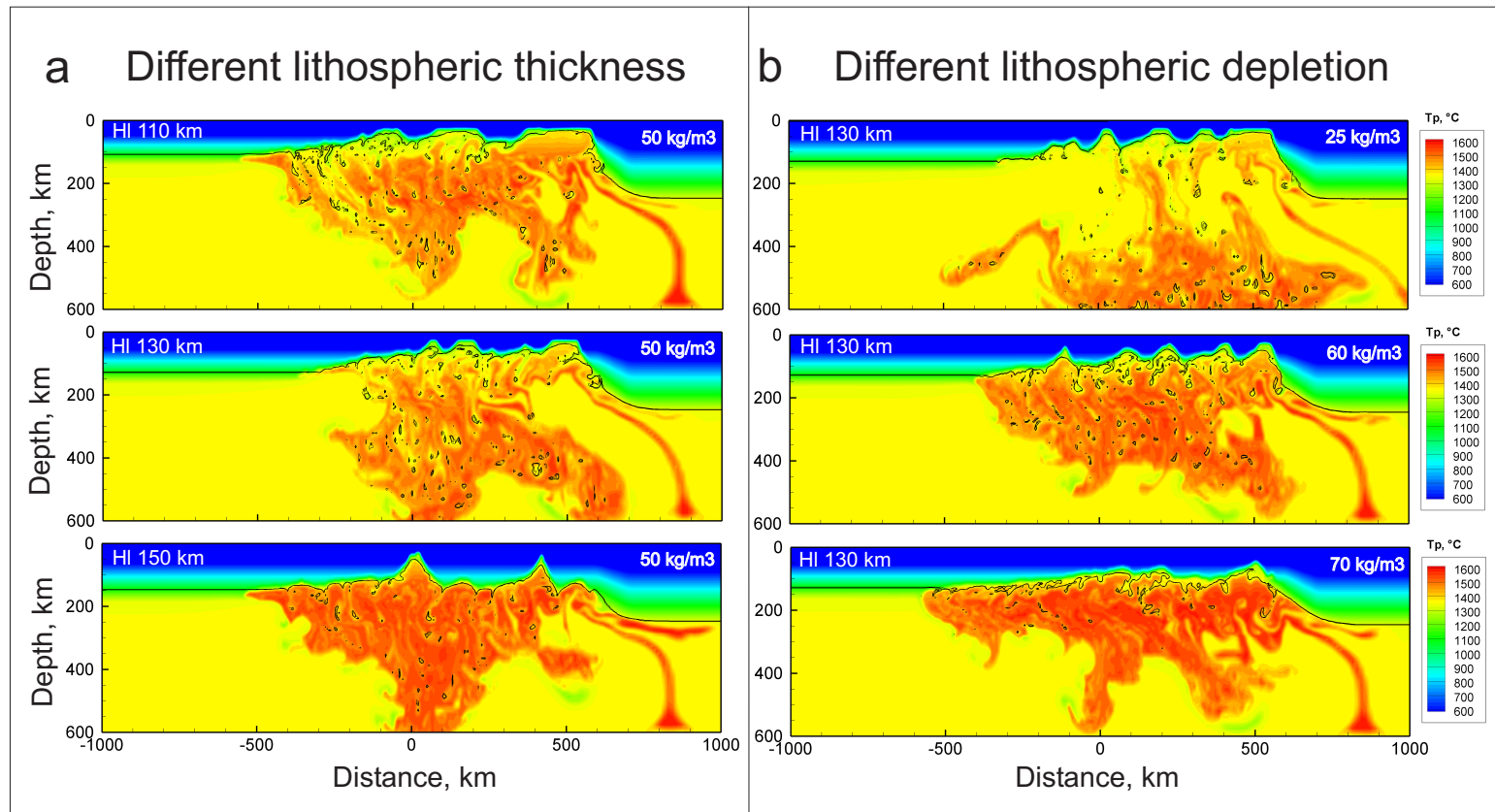


Fig. S4. Effect of thickness of the depleted lithosphere (a) and degree of depletion (b) on the intensity of the lithospheric destruction. Shown are temperature distributions at model time 1.0 Myr.

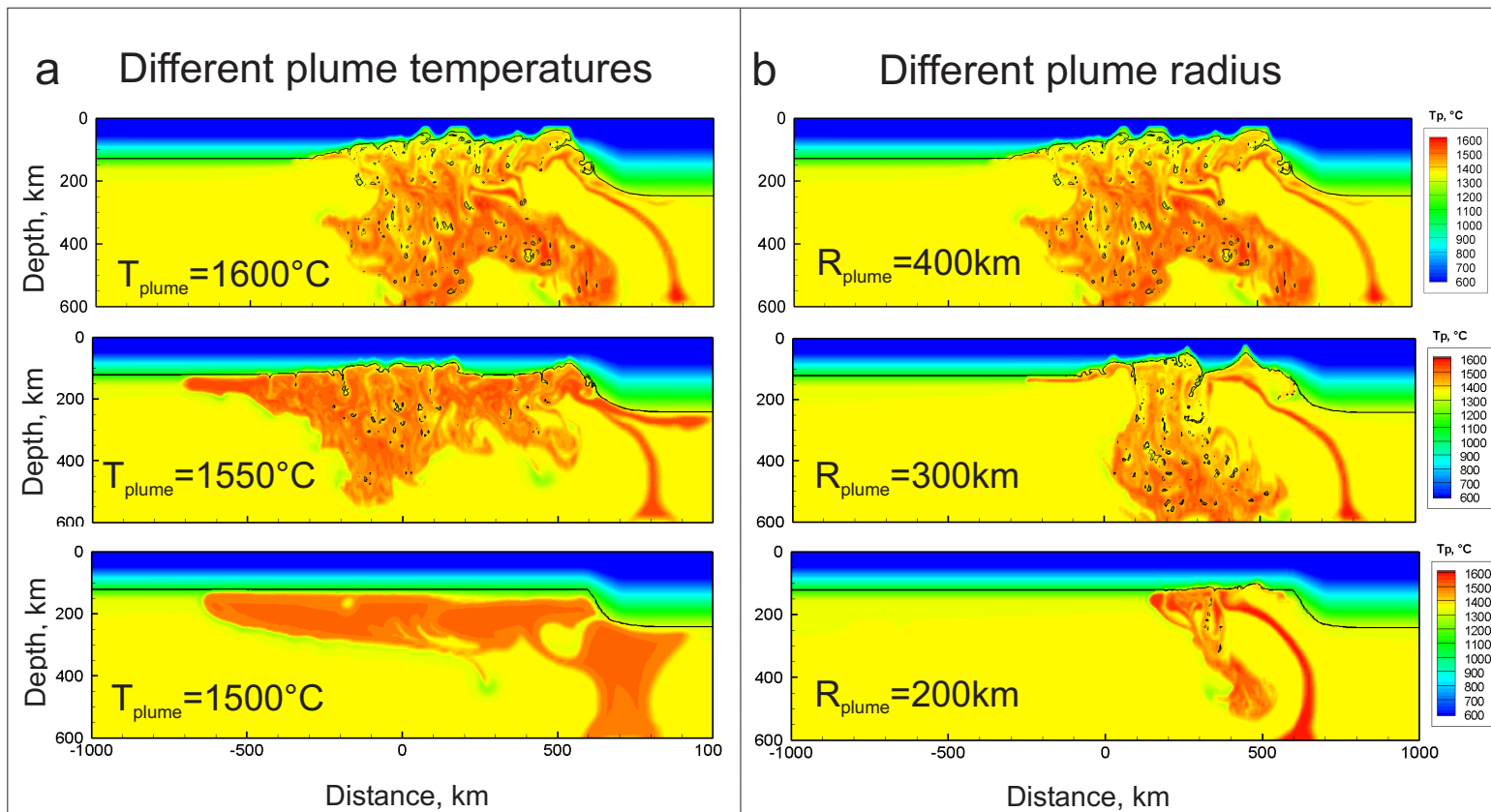


Fig. S5. Effect of a plume temperature (a) and a plume radius (b) on the intensity of the lithospheric destruction. Shown are temperature distributions at model time 1.0 Myr.

Different plume composition

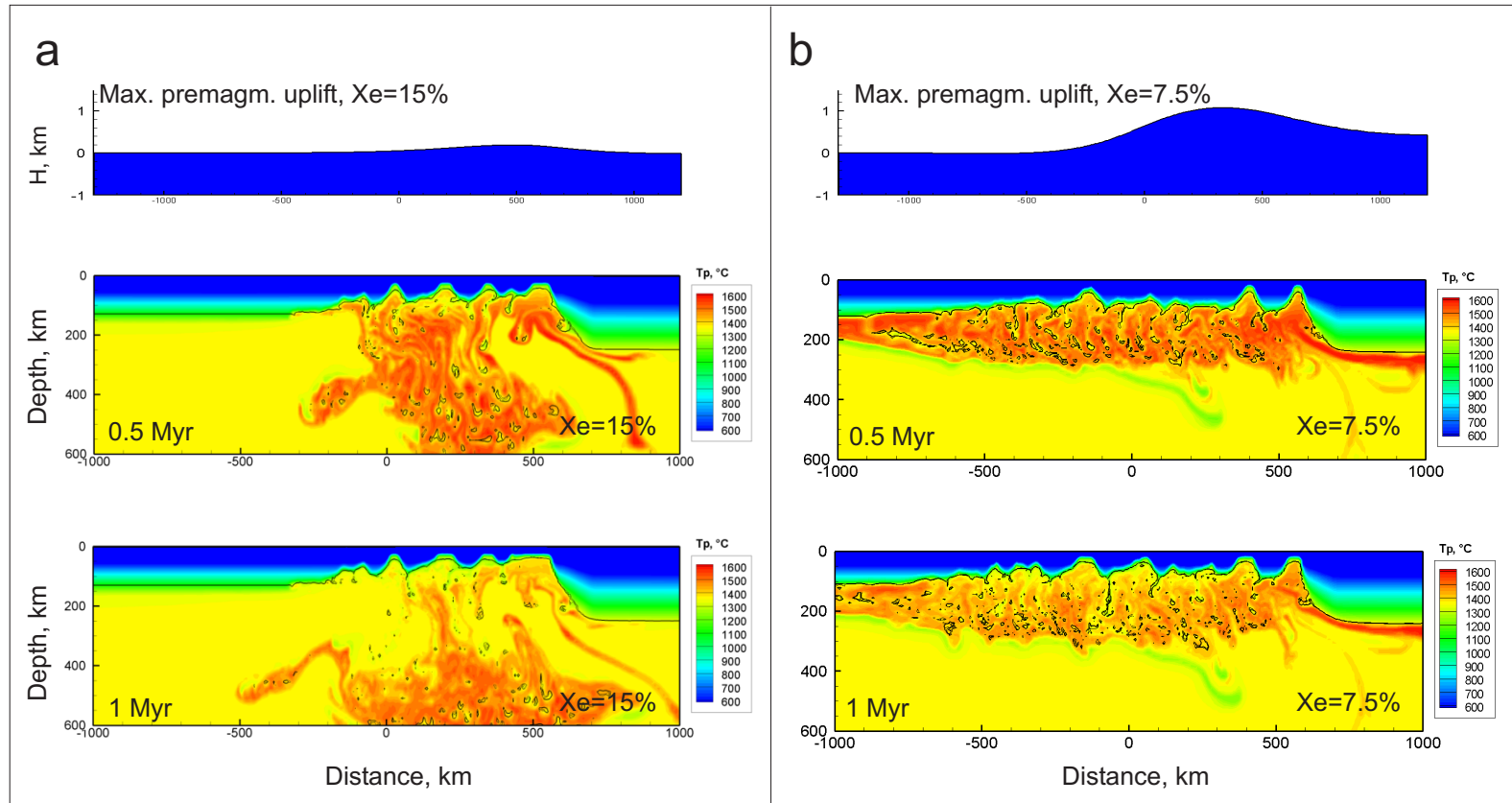


Fig. S6. Effect of a plume composition on pre-magmatic surface topography and on intensity of the lithospheric destruction. Shown is the maximum pre-magmatic surface topography (upper panel) and temperature distributions at model times 0.5 and 1.0 Myr. Content of the recycled crust component in plume is 15 Wt% (a) and 7.5 Wt% (b).